

AL-TR-90-038

AD:

2

D-A228 869

DTIC FILE COPY

Final Report
for the period
1 Aug 1986 to
31 Dec 1989

Experimental Studies of the Properties of Trihydrogen and Tetrahydrogen

October 1990

Author:
Aron Kupperman

California Institute of Technology
Pasadena, CA 91125

F04611-86-K-0076

DTIC
ELECTE
NOV 15 1990
S B D

Approved for Public Release

Distribution is unlimited. The AL Technical Services Office has reviewed this report and it is releasable to the National Technical Information Service, where it will be available to the general public, including foreign national.

Prepared for the: **Astronautics Laboratory (AFSC)**

Air Force Space Technology Center
Space Systems Division
Air Force Systems Command
Edwards Air Force Base, CA 93523-5000

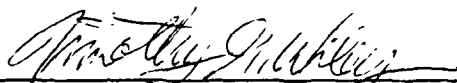
NOTICE

When U. S. Government drawings, specifications, or other data are used for any purpose other than a definitely related Government procurement operation, the fact that the Government may have formulated, furnished, or in any way supplied the said drawings, specifications, or other data, is not to be regarded by implication or otherwise, or in any way licensing the holder or any other person or corporation, or conveying any rights or permission to manufacture, use or sell any patented invention that may be related thereto.

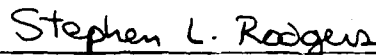
FOREWORD

This final report was submitted by California Institute of Technology, Pasadena CA on completion of contract F04611-86-K-0076 with the Astronautics Laboratory (AFSC), Edwards AFB CA. AL Project Manager Capt Tim Wiley.

This report has been reviewed and is approved for release and distribution in accordance with the distribution statement on the cover and on the DD Form 1473.



TIMOTHY G. WILEY, CAPT, USAF
Project Manager



STEPHEN L. RODGERS
Chief, Applied Research in Energy Storage
Office

FOR THE DIRECTOR



ROBERT C. CORLEY
Director, Astronautical Sciences Division

REPORT DOCUMENTATION PAGE

Form Approved
OMB No. 0704-0188

1a. REPORT SECURITY CLASSIFICATION UNCLASSIFIED			1b. RESTRICTIVE MARKINGS		
2a. SECURITY CLASSIFICATION AUTHORITY			3. DISTRIBUTION/AVAILABILITY OF REPORT Approved for Public Release; Distribution is unlimited		
2b. DECLASSIFICATION/DOWNGRADING SCHEDULE					
4. PERFORMING ORGANIZATION REPORT NUMBER(S)			5. MONITORING ORGANIZATION REPORT NUMBER(S) AL-TR-90-038		
6a. NAME OF PERFORMING ORGANIZATION California Institute of Technology		6b. OFFICE SYMBOL (If applicable)	7a. NAME OF MONITORING ORGANIZATION Astronautics Laboratory (AFSC)		
6c. ADDRESS (City, State, and ZIP Code) Pasadena, CA 91125			7b. ADDRESS (City, State, and ZIP Code) AL/LSX Edwards AFB CA 93523-5000		
8a. NAME OF FUNDING/SPONSORING ORGANIZATION		8b. OFFICE SYMBOL (If applicable)	9. PROCUREMENT INSTRUMENT IDENTIFICATION NUMBER F04611-86-K-0076		
8c. ADDRESS (City, State, and ZIP Code)			10. SOURCE OF FUNDING NUMBERS		
			PROGRAM ELEMENT NO. 62302F	PROJECT NO. 5730	TASK NO. 00WQ
11. TITLE (Include Security Classification) Experimental Studies of the Properties of Trihydrogen and Tetrahydrogen (U)					
12. PERSONAL AUTHOR(S) Kuppermann, Aron					
13a. TYPE OF REPORT Final		13b. TIME COVERED FROM 860801 TO 891231		14. DATE OF REPORT (Year, Month, Day) 9010	
15. PAGE COUNT 64					
16. SUPPLEMENTARY NOTATION					
17. COSATI CODES			18. SUBJECT TERMS (Continue on reverse if necessary and identify by block number) trihydrogen, tetrahydrogen, H ₃ , H ₄ , molecular beam metastable H ₃		
FIELD	GROUP	SUB-GROUP			
21	09				
19. ABSTRACT (Continue on reverse if necessary and identify by block number) Results of theoretical calculations by Nicolaides et al. have suggested the existence of metastable tetrahydrogen (H ₄) molecules (in the ¹ A' state). The specific impulse of this species is estimated to be 1820 s, making it a very interesting candidate for a rocket propulsion system. One possible means of producing this molecule experimentally is through the reaction H ₃ (2p ² A'' ₂) + HI(X ¹ Σ ⁺) → H ₄ (¹ A') + I(2P _{3/2}) in a crossed molecular beam apparatus. We					
20. DISTRIBUTION/AVAILABILITY OF ABSTRACT <input checked="" type="checkbox"/> UNCLASSIFIED/UNLIMITED <input type="checkbox"/> SAME AS RPT. <input type="checkbox"/> DTIC USERS			21. ABSTRACT SECURITY CLASSIFICATION UNCLASSIFIED		
22a. NAME OF RESPONSIBLE INDIVIDUAL Captain Tim Wiley			22b. TELEPHONE (Include Area Code) (805) 275-5749		22c. OFFICE SYMBOL LSX

have assembled such an apparatus. In it, the primary beam is an intense beam of long lived metastable $H_3(2p^2A_2'')$ molecules formed by an arc discharge through hydrogen. The secondary beam of HI molecules is produced by expansion through a glass capillary array. The scattered products of the $H_3 + HI$ collisions are measured with the help of an electron bombardment quadrupole mass spectrometer, having two angular motion degrees of freedom. This complex apparatus was put together and made operational. Preliminary experiments were then performed and the results indicated that it would indeed permit the proposed reaction to be investigated in detail. At this point, further more accurate calculations by Montgomery et al. found that H_4 in the $^1A'$ state is not bound. This result led us to concentrate on studying the properties of the metastable H_3 beam. Experimental work in our laboratories has resulted in the production of a high-intensity high-energy beam of metastable trihydrogen molecules (in the $2p^2A_2''$ state) whose lifetime exceeds $40 \mu s$. The specific impulse of this species is estimated to be 2050 s, and therefore another interesting candidate for a rocket propulsion system. A sophisticated apparatus to produce and characterize a metastable beam of H_3 molecules was designed, constructed and assembled. It consists of an arc heated metastable H_3 source with a translation-rotation assembly, a Stern-Gerlach magnetic velocity selector, a laser photoionization system, and an electron bombardment mass spectrometer detector. This system will be used in the future to determine the rovibrational composition, the translational energy distribution and radiative lifetime of the metastable H_3 beam and to determine its chemical properties.



Accession For	
NTIS GRA&I	<input checked="" type="checkbox"/>
DTIC TAB	<input type="checkbox"/>
Unannounced	<input type="checkbox"/>
Justification	
By	
Distribution/	
Availability Codes	
Dist	Avail and/or Special
A-1	

TABLE OF CONTENTS

1.	Scientific Background	1
1.1	Specific Impulse Considerations	1
1.2	Properties Of H_4	3
1.3	Properties Of Metastable H_3	6
1.4	Energetics And Dynamics Of The $H_3 + HI$ Reaction	10
1.5	Experimental Studies Of H_4	12
1.6	Experimental Studies Of H_3	13
1.7	Rovibrational Population Measurements	14
1.8	Translational Energy Distribution Measurements	17
1.9	Lifetime Measurements	19
2.	Equipment, Design, Construction And Testing	24
2.1	Apparatus Description	24
2.2	HI Beam Trap	30
2.3	Maintenance	31
2.4	Arc Discharge Source	31
2.5	Source Translation-Rotation Assembly	39
2.6	Arc Discharge Source Control Panels	42
2.7	Source Chamber	43
2.8	Differential Stage Chamber	49
2.9	Mass Spectrometer Vacuum Chamber	50
2.10	Mass Spectrometer	51
2.11	Laboratory	52
2.12	Laser Photoionization System	53
2.13	Computer System	54

3.	Experiments	55
4.	Conclusions	58
5.	References	59

LIST OF FIGURES

Figure 1. Schematic Representation of the $2p_z$ Rydberg orbital of H_3 molecules in the $2p_z^2 A_2''$ state	5
Figure 2. Energy level diagram for H_3	8
Figure 3. Energy levels for the $H_3 + HI$ system	11
Figure 4. Schematic horizontal cut view of the apparatus used in the rovibrational population measurements	16
Figure 5. Some of Helm's results	18
Figure 6. Schematic horizontal cut view of the apparatus used in the lifetime of H_3 measurements	20
Figure 7. Horizontal cut view of photoionization cell	21
Figure 8. Vertical cut view of photoionization cell	22
Figure 9. Schematic horizontal cut view of the apparatus used in the experiments in which the H_3 beam was tested	25
Figure 10. AC ion current as a function of m/e	27
Figure 11. Vertical cut view of the crossed molecular beam apparatus	28
Figure 12. Side view of hybrid apparatus	29
Figure 13. Cut away view of arc discharge source	32
Figure 14. Scale drawing of cathode assembly	34
Figure 15. Exploded view of anode assembly	36
Figure 16. Schematic view of the top of the source, magnet and translation assembly	38
Figure 17. Side view of translation-rotation assembly	40
Figure 18. Arc discharge source electrical control panel	44
Figure 19. Arc discharge source gas flow control panel	45

Figure 20. Horizontal cut view of apparatus used for H_3 experiments . . 47

Figure 21. Vertical cut view of apparatus used for H_3 experiments 49

1. SCIENTIFIC BACKGROUND

1.1 Specific Impulse Considerations

The fraction of the initial weight of a rocket which can be placed into earth's orbit, called the rocket's payload (P), depends on the specific impulse (ISP) and the storage density (SD) of the fuel used. The specific impulse of a fuel is the impulse per unit weight it can deliver to the rocket and the storage density is the energy of that fuel per unit weight of the storage system. The payload is an increasing function of both the ISP and SD. Current chemical fuels such as mixtures of liquid oxygen and liquid hydrogen, or aluminium perchlorate and rubber, have ISPs of the order of 400 s. On the other hand, a fuel with an ISP of 800 s and a high SD would permit putting significant payloads into geosynchronous orbit with single stage rockets, and would be highly desirable. However, even more moderate improvements in ISP without deterioration of the SD would be very worthwhile, as they could result in useful increases in payloads. Therefore, the search for high ISP and high SD fuels is a very important one for the future of rocket propulsion.

In the last five years, two interesting chemical fuel candidates having high ISP have emerged: metastable trihydrogen and metastable tetrahydrogen. These fuel candidates can liberate 180 Kcal/mole and 187 Kcal/mole respectively, when decomposing into ground electronic state molecular hydrogen. These values can be converted into ISP by the approximate expression¹

$$\text{ISP} = 265 \left(\frac{Q}{\text{Kcal/g}} \right)^{1/2} \text{ s} \quad (1)$$

where Q is the energy release per unit mass of propellant. This expression assumes a 60 to 1 expansion ratio in the exhaust, under isentropic conditions. It leads to

an ISP of about 2050 s for metastable trihydrogen and 1820 s for metastable tetrahydrogen. These ISPs exceed by far those of current rocket fuels, and if ways to utilize these species as propellants could be found, without excessive decrease in SD, a major increase in payload could result. Therefore, a vigorous effort in this direction was justified.

A characteristic of metastable trihydrogen (in the $2p_x^2A_2''$ electronic state) which makes it worthy of careful investigation, in addition to its high energy content of 180 Kcal/mole, is a lifetime no smaller than $40\mu s^2$ in a collision-free environment. What this lifetime actually is and how it is affected by collisions is a very important topic for study. A second important characteristic is that a method has been developed for producing a very intense beam of this species,^{2,3} of the order of 10^{20} to 10^{21} molecules s^{-1} sterad $^{-1}$. This intensity permits one to perform many important experiments designed to measure and understand its spectroscopic and dynamic properties. Such experiments are the first step towards assessing its potential, or that of related metastable molecules, as a rocket fuel, as an ingredient of a high energy laser, or, because of its high energy density, as a system useful in other presently unspecified applications. In addition, this species is of great scientific interest because of its unusual characteristics. Its low ionization potential of 3.67 eV^{4-7} permits it to react with high electronegativity species by charge transfer mechanisms. It can also act as a source of hydrogen atoms and react covalently with other molecules containing atoms which form strong bonds with H. Finally, it may be capable of attaching to other species X to form electronically excited H_3X which may still be metastable. As a result of these possibilities, it may display a rich spectrum of dynamical behaviors, possibly leading to an increase in our understanding of the reactivity of excited states.

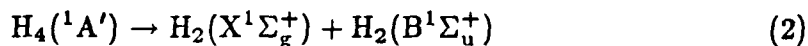
Metastable tetrahydrogen, in the $^1A'$ state, had been predicted by theoretical calculations using the maximum ionicity excited state (MIES) approach⁸. Its

assumed metastability was due to the presence of avoided crossings in the excited state potential energy surfaces, and the fact that at the equilibrium geometry of this state its energy should be lower than that of any other state. This species had not yet been detected experimentally, but an initial effort in that direction was being conducted in our laboratory when the current project started⁹. This effort was based on the study of the products of the reaction of H_3 ($2p_z^2 A_2''$) with either HI or DI in a crossed molecular beam configuration. The products could include metastable H_4 or H_3D or their dissociation products H_2 or HD , and the angular distribution of the latter would give a first experimental indication of the lifetime of tetrahydrogen. The object of this contract was to perform experiments to detect and measure the lifetime of metastable H_3 and H_4 .

1.2 Properties Of H_4

The first report of the possible existence of metastable tetrahydrogen molecules comes from the theoretical calculations of Nicolaides et al.⁸ Using the MIES approach to the calculation of electronic energies, they were able to show that due to the presence of avoided crossings, the lowest $^1A'$ potential surface for H_4 has a relatively deep well. The equilibrium configuration of that well was predicted to have the following main characteristics:

- The process



is endoergic by 3.1 eV.

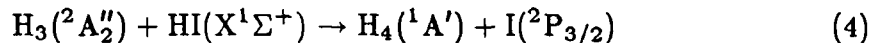
- The dissociation along the $H_3 \dots H$ direction is endoergic by 1.86 eV.
- The process



is exoergic by 8.1 eV.

- Its structure is that of a trigonal pyramid whose base is an equilateral triangle with side 1.7 bohr (only slightly larger than the 1.63 bohr value of the $2p_z^2\text{A}_2''$ state of H_3 and the 1.66 bohr value for the ground state of H_3^+) and a height of 4.0 bohr (which is comparable to the dimensions of the $2p_z$ orbital depicted in Figure 1).
- There are no other electronic states at lower energy for that equilibrium configuration, and its decomposition into two ground state H_2 molecules would have to occur by predissociation. Its predissociation lifetime had not been calculated by the time this contract started.
- It had not been detected experimentally at the time this contract started.

Due to its high specific impulse, estimated theoretically to be 1820 s, it was considered to be very important to try to determine the existence of metastable H_4 experimentally. For this project we proposed a preparation scheme based on the reaction



in a crossed molecular beam apparatus. This required a beam of metastable H_3 molecules, which we had available.

The work of Nicolaides et al.⁸ stimulated further theoretical calculations which disagreed with their results. Montgomery et al.¹⁰ performed *ab initio* calculations on H_4 using the 6s1p/4s1p basis of Nicolaides et al. and a more accurate 10s3p/5s3p basis. Using the GAUSSIAN 82 system of programs,¹¹ they found

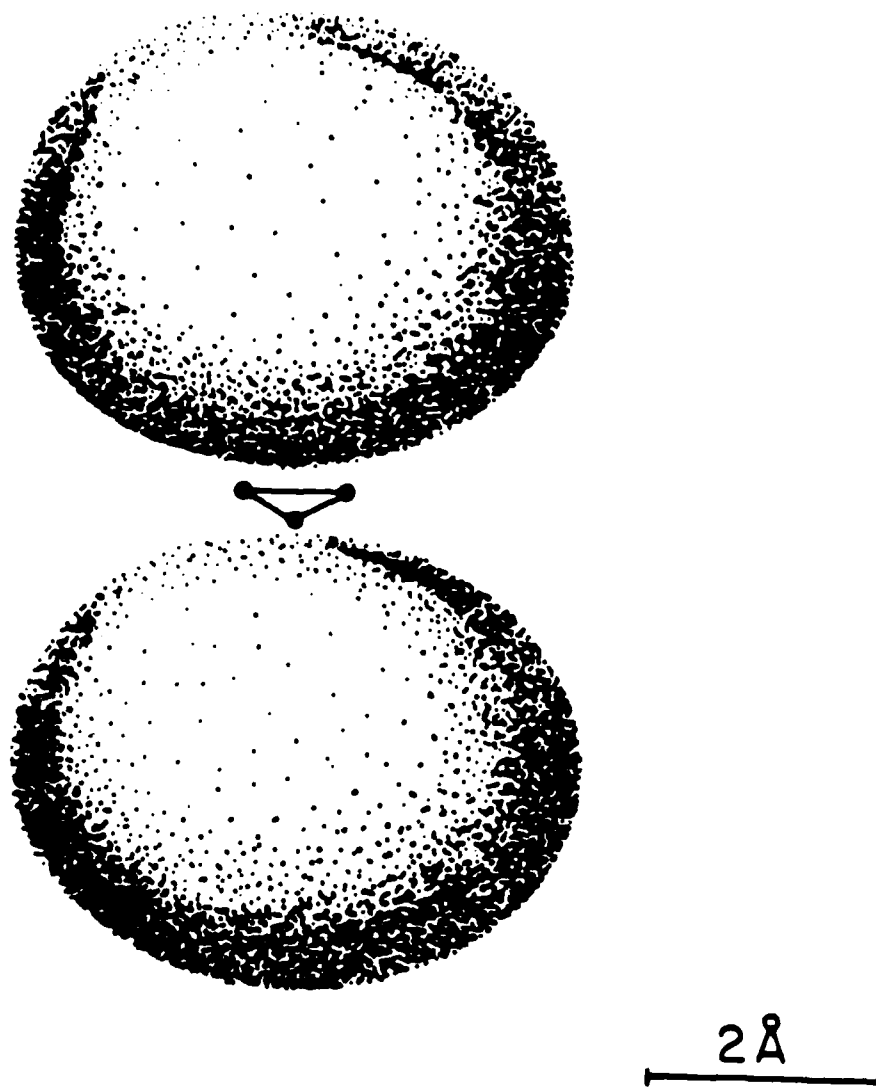


Figure 1. Schematic representation of the $2p_z$ Rydberg orbital of H_3 molecules in the $2p^2 A_2''$ state. The heavy points represent the experimentally determined equilibrium configuration¹², represented in a perspective drawing. The Rydberg orbital perpendicular to the plane of the nuclei is represented by a 90% boundary surface of a hydrogenic $2p_z$ orbital¹³.

C_{3v} optimized structures at the SCF, MP2, and CISD levels of theory using the 6s1p/4s1p basis, and the SCF and MP2 levels using the 10s3p/5s3p basis. (Note that, in pure C_{3v} symmetry, the two $^1A'$ states discussed by Nicolaides et al. correlate to the ground $^1A'$ and an excited 1E state. Since these states are of different symmetry, there is no avoided crossing in C_{3v} symmetry to stabilize the excited state, as there is in the lower C_s symmetry.) At each optimized geometry, they also performed a vibrational frequency analysis. Their results showed that the H_4 energy minima found in C_{3v} symmetry represents a saddle point, and is therefore not stable with respect to geometric perturbations which lower the spatial symmetry. Thus the ground $^1A'$ state of H_4 in C_{3v} is not bound. Since this information was not known at the outset of this project, much work was done in an attempt to detect H_4 experimentally. After publication of the work on the stability of H_4 by Montgomery et al.¹⁰, we revised the activity plan for the rest of the project, concentrating on studying the properties of the metastable H_3 beam.

1.3 Properties Of Metastable H_3

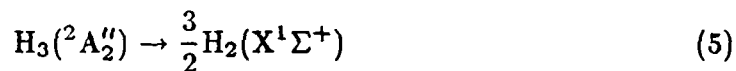
The first report of the existence of a metastable form of H_3 comes from the work of Devienne and coworkers^{14,15}, in which a beam of H_3^+ , having energies in the KeV range, is neutralized by charge exchange and subsequently reionized and detected mass spectrometrically. Variations of this technique have since been used by Gray and Tomlinson¹⁶, Barnett and Ray¹⁷, Nagasaki et al.¹⁸, Castro de Faria et al.¹⁹, Gaillard et al.²⁰, Vogler²¹, Cisneros et al.²², Gellene et al.^{23,24}, Figger et al.²⁵ and Helm et al.⁴⁻⁷. In some of these, evidence for a long lived H_3 state was found and in others not.

The first spectroscopic measurements of the electronic structure of H_3 comes from the work of Herzberg and coworkers¹². They detected, by analyzing the

light emitted from the cathode and anode regions of a glow discharge through H_2 , visible light which could be assigned to Rydberg excited states. The longest lived of these states, as inferred from the narrowness of the lines ending on it, was the $2p_z^2 A_2''$ state, whose coupling to the ground repulsive $2p^2 E'$ state was both electronically and vibronically forbidden. An energy level diagram including the Rydberg excited states of H_3 and the levels of $E(X^1 \Sigma_g^+)$ with $n = 1, 2, 3$ and ∞ are given in Figure 2.

Using a DC arc discharge through hydrogen²⁸, we were able to produce in our laboratory, under appropriate source conditions, an intense beam of $H_3(2p_z^2 A_2'')$ molecules^{2-3,29}. The main characteristics of the trihydrogen in this beam are

- A lower limit to its lifetime is $40 \mu s$.
- Its translational energy distribution function spans the range from about 0.1 eV to about 15 eV, with a maximum at about 8 eV (when the pressure in the discharge is 70 Torr).
- Its intensity is in the range of 10^{20} to 10^{21} molecules s^{-1} sterad $^{-1}$, its current density at the detector is 10^{16} to 10^{17} molecules $cm^{-2} s^{-1}$, its flux into the detector is 10^{15} to 10^{16} molecules s^{-1} , the corresponding number density is 4×10^9 to 4×10^{10} molecules cm^{-3} and the associated equivalent pressure (at 300 K) is 10^{-7} to 10^{-6} Torr.
- The exoergicity of the net process



is about 180 Kcal/mole (7.8 eV/molecule).

- Its equilibrium configuration is an equilateral triangle whose side measures 1.63 bohr, which is slightly smaller than the value of 1.66 bohr for the ground state of H_3^+ .

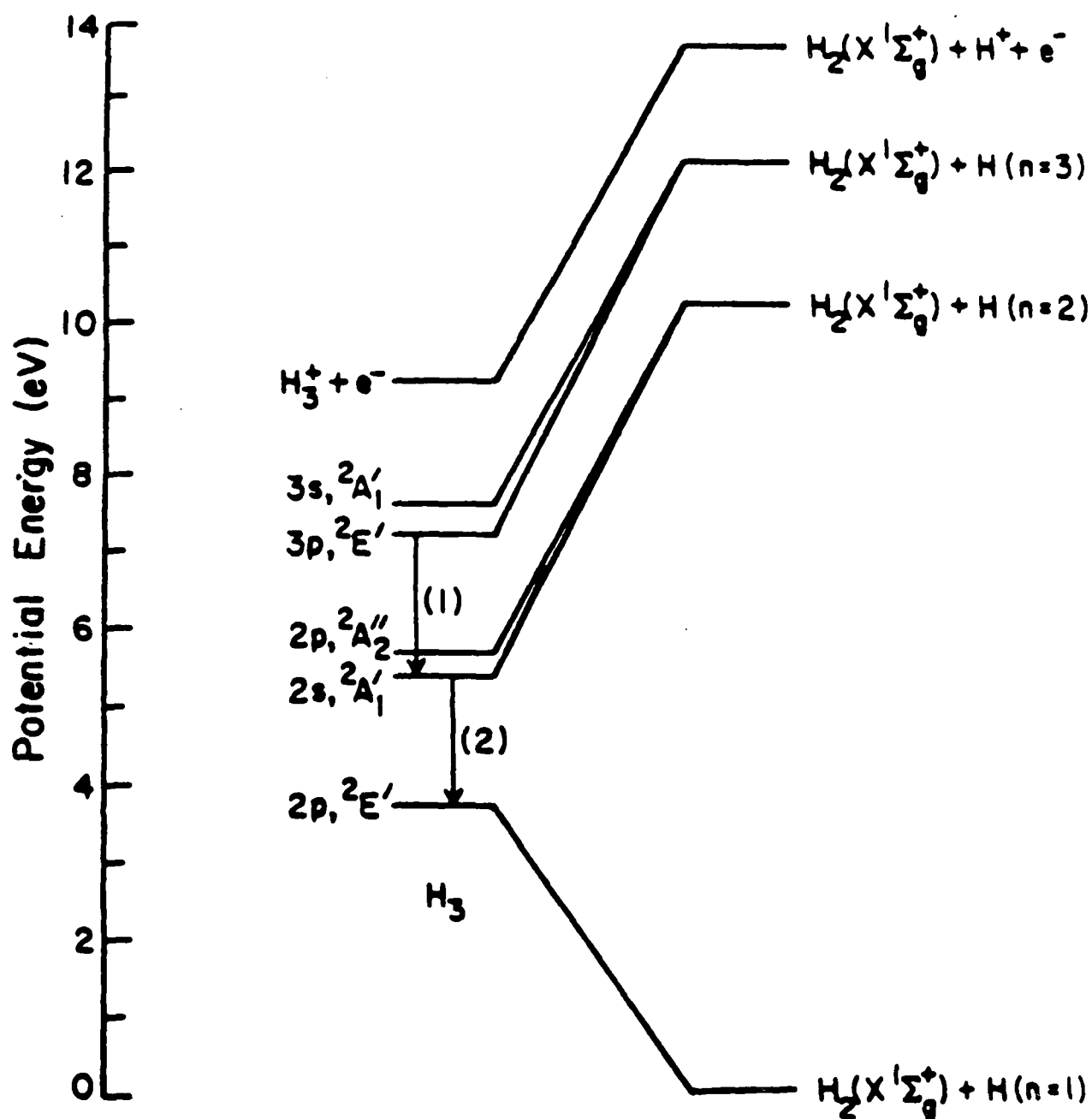


Figure 2. Energy level diagram for H_3 . the spacing of the H_3 energy levels was obtained for an equilateral triangle configuration²⁶ and referred to the energy of dissociated products by the results of a separate calculation²⁷.

- Its cross section for scattering by Ar is about 10 times larger than that of H by Ar.

The work of Herzberg et al.¹² stimulated theoretical calculations^{26,30-35} which have successfully described the spectra he observed. The conclusion of these calculations is that the Rydberg electron for the $2p_z^2A_2''$ state is in a $2p_z$ hydrogenic orbital perpendicular to the plane of the equilateral triangle H_3^+ ground state ion core. The 90% contour surface for the probability density of such an orbital in atomic hydrogen¹³ is depicted in Figure 1, superimposed on the perspective drawing of the equilateral triangle representing the equilibrium position of the nuclei in H_3 . It can be seen from this figure that the $2p_z$ orbital extends significantly beyond the three protons, and that the cross sections for H_3 undergoing different kinds of dynamic processes may turn out to be substantial, as indeed has been verified experimentally in limited cases¹². Furthermore, the lack of vibronic coupling between the $2p_z^2A_2''$ state of H_3 and its ground state $2p^2E'$ state is in part associated with the fact that the Rydberg electron $2p_z$ orbital is perpendicular to the H_3^+ ion core plane. The channels available for the decay of that state are therefore: a) radiative transition to the neighboring $2s^2A_1'$ state, which lies in the infrared and has been crudely estimated to be $87 \mu s^{24,26}$ and more accurately estimated by Helm to be $94 \mu s^{36}$ but is not really known; b) rovibrational coupling to the ground state, resulting in rovibronic predissociation.

The fact that the lifetime of H_3 ($2p_z^2A_2''$) exceeds $40 \mu s^2$ makes it possible to use it as a reagent to attempt to sample the H_4 ($^1A'$) configuration according to reaction (4).

1.4 Energetics And Dynamics Of The $H_3 + HI$ Reaction

The dissociation energy of HI (measured from the bottom of its ground state potential energy curve) is 3.2 eV. From this value and the energetics of the H_3 and H_4 systems described in Sections 1.1 and 1.2, we estimate reaction (4) to be endoergic by 1.0 eV. Some of the energetics of these systems is depicted in Figure 3. The fact that, as mentioned in Section 1.2, our H_3 ($2p_z^2A_2''$) beam has a maximum in its translational energy distribution function at an energy of 8 eV makes the endoergicity of reaction (4) easy to overcome from an energy point of view.

The determining factor of whether reaction (4) does or does not occur is therefore the dynamics of the system. Part of this dynamics is determined by geometrical considerations. As pointed out in Sections 1.1 and 1.2, the equilibrium geometries of H_3 ($2p_z^2A_2''$) and of the base of the H_4 ($^1A'$) pyramid are very similar. They are both equilateral triangles, whose sides measure 1.63 bohr and 1.7 bohr respectively. In addition, the centers of the $2p_z$ Rydberg orbital lobes in H_3 ($2p_z^2A_2''$) are located about 4.2 bohr above and below the H_3^+ ion core plane, as can be seen from Figure 1. This is to be compared with the height of 4.0 bohr of the triangular pyramid which represents the equilibrium configuration of H_4 ($^1A'$). Therefore relatively little distortion in the H_3 ($2p_z^2A_2''$) reagent is required for reaction (4) to take place. What is required is a simple transfer of an atom from the HI molecule to the region of the Rydberg orbital of the H_3 ($2p_z^2A_2''$) molecule. This seems to be dynamically not too difficult.

The total scattering cross section of H_3 ($2p_z^2A_2''$) by HI should be about 10 times larger than that of H by HI, on the basis of the relative cross sections for $H_3 + Ar$ and $H + Ar$ mentioned in Section 1.2. It is more difficult to estimate the ratio of the corresponding reaction cross sections, but the ratio of the H_3 and H sizes is in favor of the former process. Furthermore, the $H + HI$ reaction cross

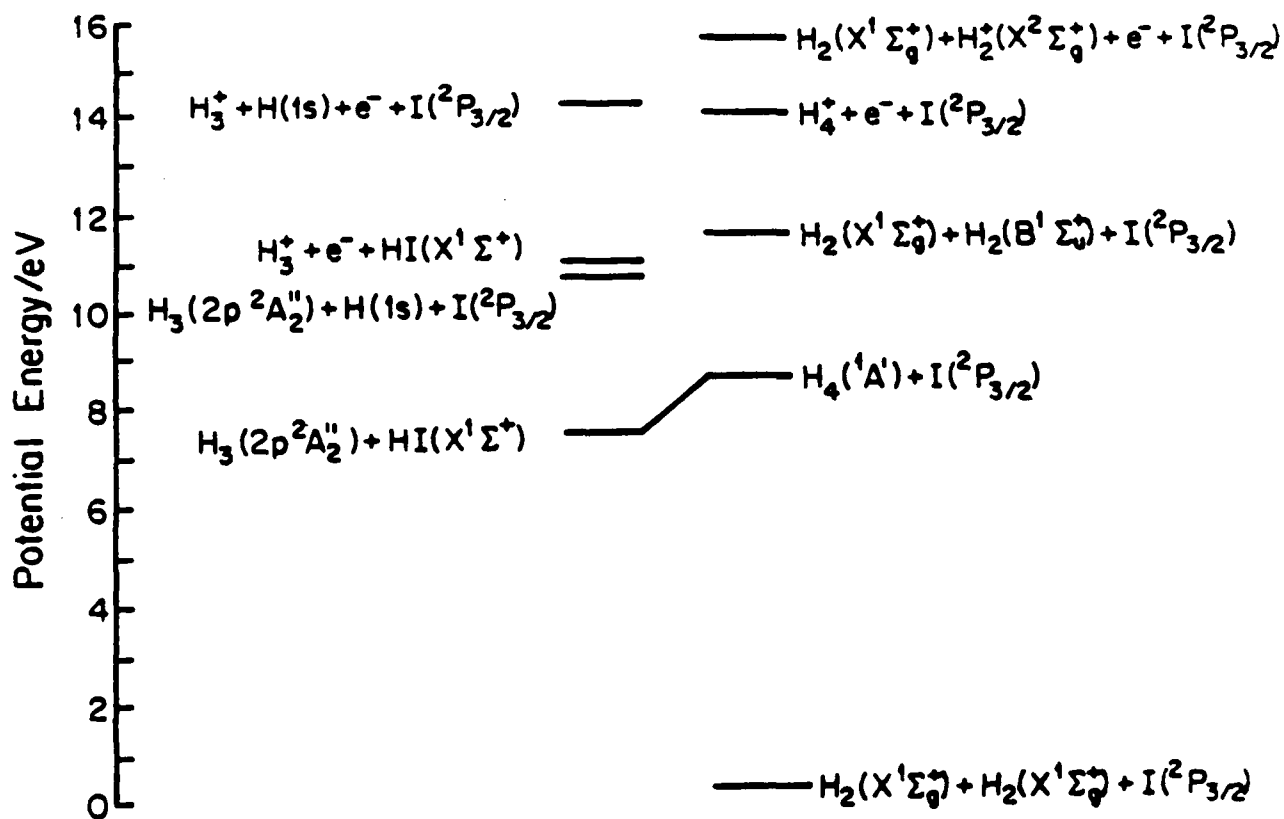
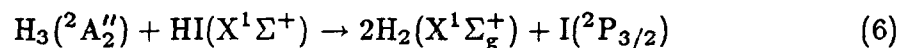


Figure 3. Energy levels for the $H_3 + HI$ system.

section at thermal energies is of the order of 1 \AA^2 . Therefore, if this species were metastable and had the characteristics originally predicted, reaction (4) would be a good first candidate for the preparation of H_4 ($^1\text{A}'$).

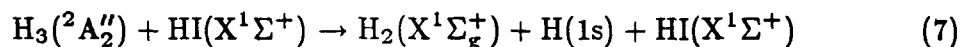
1.5 Experimental Studies Of H_4

A reaction which might compete with (4) is

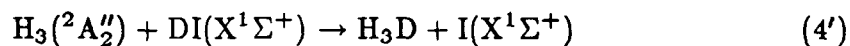


This reaction is exoergic by about 7.3 eV, but involves a large electronic nonadiabaticity as well as the concerted formation of 3 products. As a result, reaction (6) may not preclude the occurrence of reaction (4), whose cross section might still be of the order of 1 \AA^2 or more, at the translational energies considered. Such a cross section would be adequate for the experimental measurement of that process in our apparatus, given the large H_3 beam intensity and energy available. A more serious difficulty would be the verification of the occurrence of reaction (4), given the probable short lifetime of the H_4 ($^1\text{A}'$) species. Nevertheless, if that lifetime were of the order of 10^{-9} s or longer, the H_4 would undergo about 10^3 rotations or more before dissociating, probably into two H_2 molecules. These dissociation products would, as a result, exhibit an angular distribution which is broad and symmetric about 90° in the center of mass frame³⁷. On the other hand, if reaction (6) occurs and is, as expected, a direct reaction (since no strongly attractive wells are expected to exist in the $\text{H}_3(2p_z^2\text{A}_2'') + \text{HI}(\text{X}^1\Sigma^+)$ potential energy surface), such symmetry would not be exhibited. We could therefore use the details of the angular distribution of the H_2 products as a diagnostic for the occurrence of reaction (4). Such a diagnostic would be useful as long as the H_4 ($^1\text{A}'$) species lived for a few rotations (i.e., about 10^{-12} s) or longer.

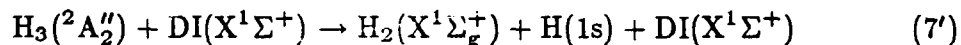
In order to distinguish between reaction (4) and the collision induced dissociation process



we could replace the HI by DI. The reactions corresponding to (4) and (7) now become



and



If the H_3D formed dissociated into two hydrogen molecules, they would be H_2 and HD , whereas (6') cannot produce HD products. The HD detected could be distinguished from elastically scattered H_3 reagent by its angular distribution. A Newton diagram analysis shows that, because of the large H_3 laboratory velocity, the elastically scattered H_3 would be forward peaked, appearing at small laboratory scattering angles with respect to the incident laboratory H_3 beam, whereas, as mentioned above, the HD resulting from the dissociation of H_3D was expected to have a broad angular distribution symmetric around 90° in the center of mass frame. This was the original plan for investigating H_4 or its isotopically substituted counterpart H_3D .

1.6 Experimental Studies Of H_3

In order to understand the reason behind the long lifetime ($> 40\mu\text{sec}$) of metastable the H_3 molecules in our beam, it would be very useful to determine

the rovibrational population distribution, as well as the radiative lifetimes of the magnetic-dipole transition and electric-quadrupole transitions from the $2p_x^2A_2''$ electronic state to the ground $2p^2E'$ electronic state, and the lifetime of the electric-dipole transition from the $2p_x^2A_2''$ electronic state to the excited $2s^2A_1'$ electronic state. The longest lived ro-vibronic states of the $2p_x^2A_2''$ electronic state of the H_3 molecule are expected to be those having no rotational energy, and varying amounts of vibrational energy. This is due to the fact that the decay of the $2p_x^2A_2''$ electronic state must occur through predissociation to the ground state which can occur only through rovibronic coupling, or by one of the other above mentioned processes.

1.7 Rovibrational Population Measurements

As shown by Helm,⁴⁻⁷, the rovibrational population measurements can be done with the help of a coaxial dye laser in counter current with the H_3 molecular beam. The laser is tuned so as to excite transitions to high- n Rydberg states of H_3 . The excited molecules then either autoionize, or are electric field ionized. The resulting H_3^+ ions are then detected mass spectrometrically.

The rovibrational population measurements will be performed using the experimental set-up depicted in Figure 4 . The experiment consists of producing and intense beam of H_3 molecules. Ions are swept out of the beam path by the electric field produced by deflection plates (D). Beyond this point, the beam consists of only neutral species. The beam is then crossed with a 20 Hz coaxial dye laser in counter current with the beam. The laser light is tuned to excited transitions to high- n Rydberg states ($7 < n < 40$) of the H_3 molecule. To produce excitation to these Rydberg states requires scanning the laser wavelength over the

range from ~ 335 - 370 nm. Over this range the dye laser provides pulse energies of typically 8 - 10 mJ. The 10 ns laser pulses have a spectral width of ~ 0.5 cm^{-1} .

Detectable excitation will take place beginning after the first set of deflection plates (D) up to the field ionization plates (IL). High- n Rydberg states of atoms and molecules are easily and efficiently ionized by a DC electric field of the appropriate strength. The ions produced are then mass analyzed. During these measurements, the mass spectrometer is operated with the ionizer off, since we are only interested in detecting the molecules ionized by the field ionization following laser excitation. The electron multiplier output is counted over a time window beginning about 200 ns following the laser pulse and ending after 2.5 μs (corresponding to the flight time of the 8 eV H_3 molecules over the field free flight path between (D) and (IL)).

Some of the vibrational bands in these electronic transitions have already been tentatively assigned by Helm.^{4,6,7} He was able to assign transitions belonging to five Rydberg series which he labelled A, B, B', C and D. Of noteworthy importance is that in Helm's observation of longlived metastable H_3 produced by other means than ours, the initial electronic state of the molecules was $2p_z^2A_2''$ and that the molecules were all in the ground rotational state with varying amounts of vibrational energy. This is also what is expected in our beam. However, it is likely that there will be more vibrational excitation in our beam due to the manner in which it is produced.

Helm found that the line positions in these series could be represented with a precision better than 0.5 cm^{-1} using the following expression

$$E_n = T_\infty - \frac{R}{(n - \delta_{\text{eff}})^2} \quad (8)$$

where $R = 109717.39$ cm^{-1} . A fit of this data to the spectra he observed yielded the series limits T_∞ and effective quantum defects δ_{eff} listed in Table 1 of Figure 5.

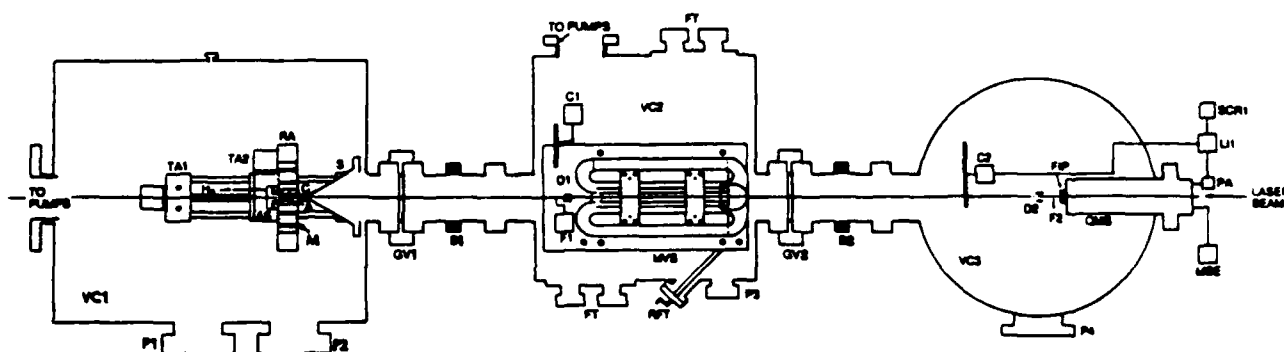


Figure 4. Schematic horizontal cut view of the apparatus that will be used in the rovibrational population experiments VC1, VC2 and VC3, vacuum chambers; AS, anode assembly; A, anode; C, cathode; M, magnet; S, water-cooled copper skimmer; TA1 and TA2, translation assembly; RA, rotation assembly; P1, P2, P3 and P4, viewports; GV1 and GV2, gate valves; B1 and B2, flexible bellows; MVS magnetic velocity selector; FT, feedthroughs; RFT, rotary feedthrough; C1 and C2, choppers; D1 and D2, electric field deflector plates; F1 and F2, mechanical flag; FIP, field ionization plates; QMS, quadrupole mass spectrometer; PA, preamplifier; MSE, mass spectrometer electronics; LI1, lock-in amplifier; SCR1, strip chart recorder.

Also shown in this figure are the spectra he observed and tentative assignments made. This information will facilitate the interpretation of our results.

The variation in the rovibrational population with changing source conditions will be examined in order to maximize the intensity of those states which are apt to have the longest predissociation lifetimes. This optimization will be useful for subsequent experiments discussed below.

1.8 Translational Energy Distribution Measurements

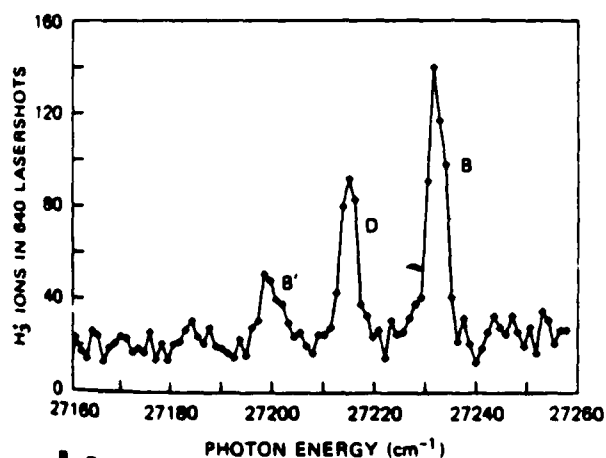
The translational energy distribution measurements will be performed using the experimental set-up depicted in Figure 4. A Stern-Gerlach magnetic velocity selector, housed in the differential stage chamber, will be used to determine the translational energy distribution of the H_3 beam. The intensity of this beam at the exit of the magnet, with the magnet set at a resolution of 0.1 to 0.2 eV, is expected to be in the range of 10^{16} to 10^{17} molecules sterad $^{-1}$ s $^{-1}$ and the corresponding flux into the mass spectrometer detector 10^{11} to 10^{12} molecules s $^{-1}$. The rovibrational population of this translationally selected beam will then also be determined. These intensities are sufficiently high to permit such measurements. By scanning the magnetic field in the Stern-Gerlach velocity selector, the translational energy distribution function of each of the vibrational states identified, all of which are expected to be rotationless, will be determined. This will provide the detailed translational-internal energy distribution function of the metastable trihydrogen molecules of our beam, and will completely characterize it. This dependence will then be determined as a function of the arc source conditions to maximize our understanding and control of this beam.

a)

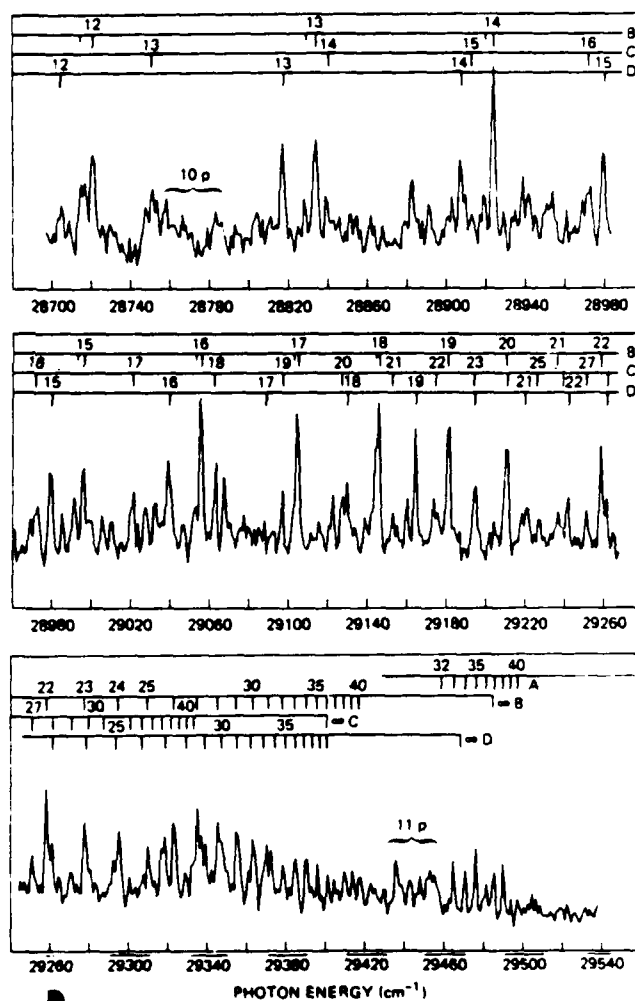
TABLE I. Observed Rydberg series of H_3 molecule. The state designation is (ν_1, ν_2, N, K) for the lower state and (ν_1, ν_2, N^*, G) for the H_3^+ core.

Series	$\tilde{B} 2p^2 A_2''$	Upper state H_3^+ core	T_∞ (cm^{-1})	δ_{eff}	Observed n range
A	(0,0,0,0)	(0,0,1,0)	29 566.0	*	32-40
B	(0,1,0,0)	(0,1,1,1)	29 485.5	0.022	7,8,12-40
B'	(0,1,0,0)	(0,1,1,1)	29 485.5	0.073	7,12-32
C	(...)	(...)	29 402.0	0.02	13-36
D	(1,0,0,0)	(1,0,1,0)	29 469.5	0.02	7,12-32

*When series A is fitted together with the $R0 (3s-2p)$ transition (Ref. 2) a value $\delta_{eff}=0.0803$ is obtained. When fitted together with the $R0 (3d-2p)$ transition (Ref. 5) $\delta_{eff}=0.0095$ is obtained.



b) Excitation spectrum of $n=7$ states of H_3 .



c)

Excitation spectrum of high- n states of H_3 . Four series are marked in the top of the figure. The series B' is indicated by the small tick marks along with series B .

Figure 5. Summary of Helm's results

1.9 Lifetime Measurements

In order to determine whether or not this intense beam of H_3 molecules could be used in various applications, a better estimate of its lifetime is required. Although radiative transitions from the $2p_z^2A_2''$ electronic state to the ground $2p^2E'$ electronic state are electric-dipole forbidden, they are magnetic-dipole and electric-quadrupole allowed. The corresponding lifetimes are expected to be of the order of 10^{-3} s and 1 s respectively.³⁸

The radiative lifetime measurements will be performed using the experimental set-up depicted in Figure 6. The experiment consists of producing an intense beam of H_3 molecules. Ions as well as highly excited Rydberg states of H_3 molecules are swept out of the beam path by the electric field produced by the deflection plates (DP). Beyond this point, the beam consists of only neutral H_3 molecules in their $2p_z^2A_2''$ electronic state. Other higher lying Rydberg states of H_3 , as discussed previously, are expected to have lifetimes less than $10 \mu s^{39-41}$ and therefore will have already decayed to the $2p_z^2A_2''$ electronic state or to the ground $2p^2E'$ electronic state and have dissociated. Any emission which occurs beyond the deflection plates will be due to the decay of the $2p_z^2A_2''$ electronic state of H_3 . This intense beam of H_3 molecules is then passed through a cell similar to the design of the cell shown in Figures 7 and 8. By viewing the light emitted by the H_3 beam as it traverses the cell a better estimation of the radiative lifetime of this state will be obtained. Attempts to use this cell in the past have failed due to the large photon background in the chamber. To eliminate this problem, the design of the cell was modified.

Several changes in the cell design will be implemented. The entrance and exit of the cell will be baffled to eliminate background light emanating from the source and chamber as much as possible. A monochromator will be used

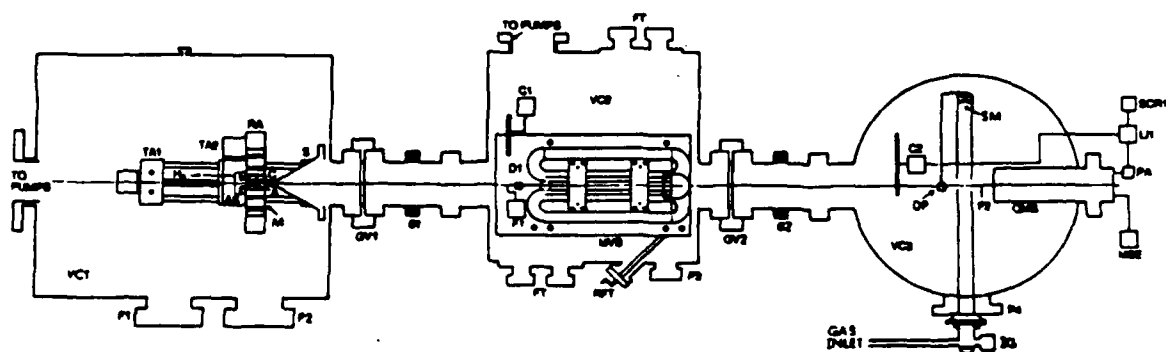


Figure 6. Schematic horizontal cut view of the apparatus used in the lifetime measurements VC1, VC2 and VC3, vacuum chambers; AS, anode assembly; A, anode; C, cathode; M, magnet; S, water-cooled copper skimmer; TA1 and TA2, translation assembly; RA, rotation assembly; P1, P2, P3 and P4, viewports; GV1 and GV2, gate valves; B1 and B2, flexible bellows; MVS magnetic velocity selector; C1 and C2, choppers; D1 and D2, electric field deflector plates; F1 and F2, mechanical flag; FT, feedthroughs; RFT, rotary feedthrough; DP, electric field deflectors; SM, spherical mirror; IG, ion gauge; QMS, quadrupole mass spectrometer; PA, preamplifier; MSE, mass spectrometer electronics; LI1, lock-in amplifier; SCR1, strip chart recorder.

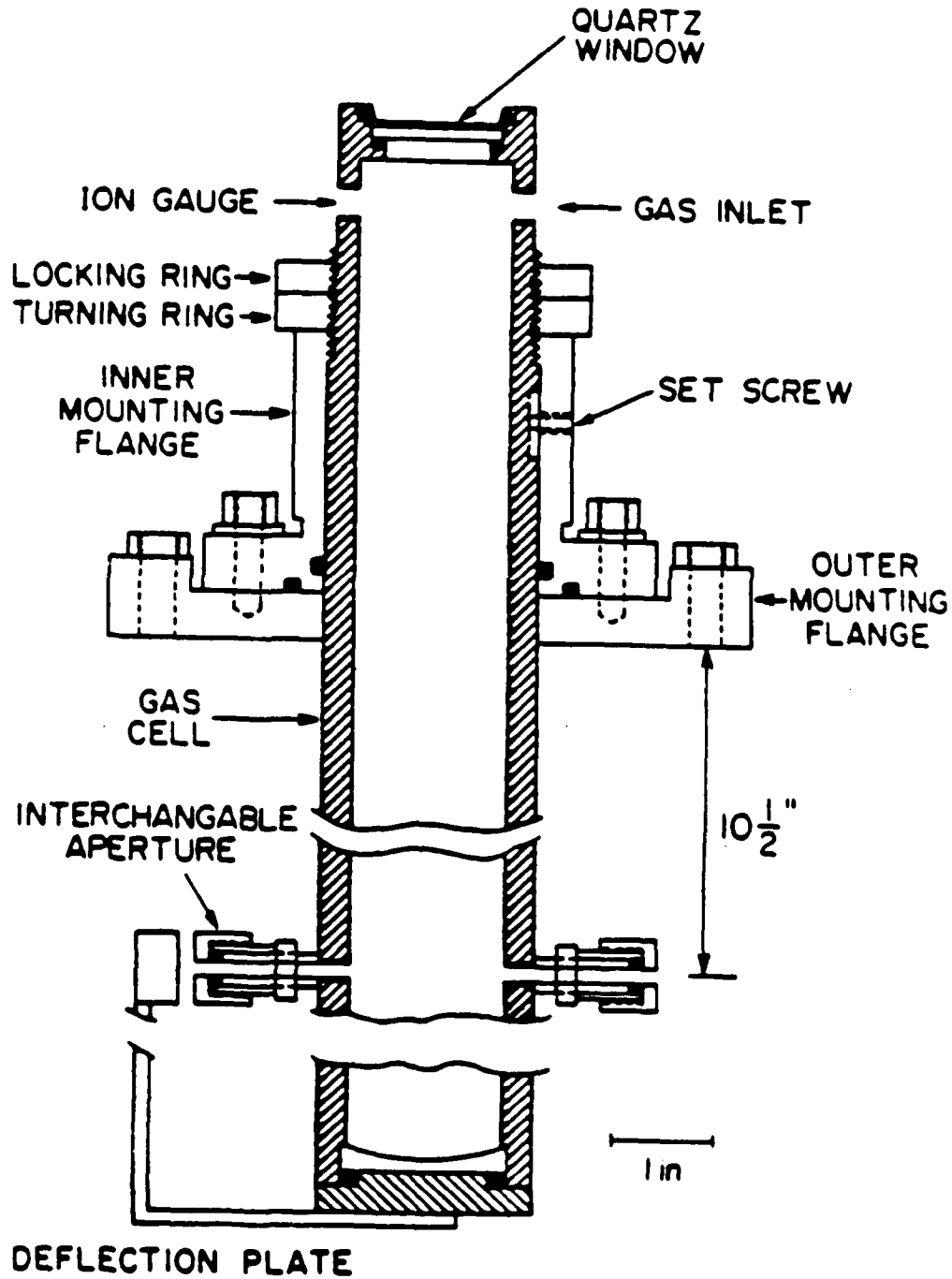


Figure 7. Horizontal cut view of photoionization cell with mounting flange.

Hatched area of drawing indicates the pipe walls.

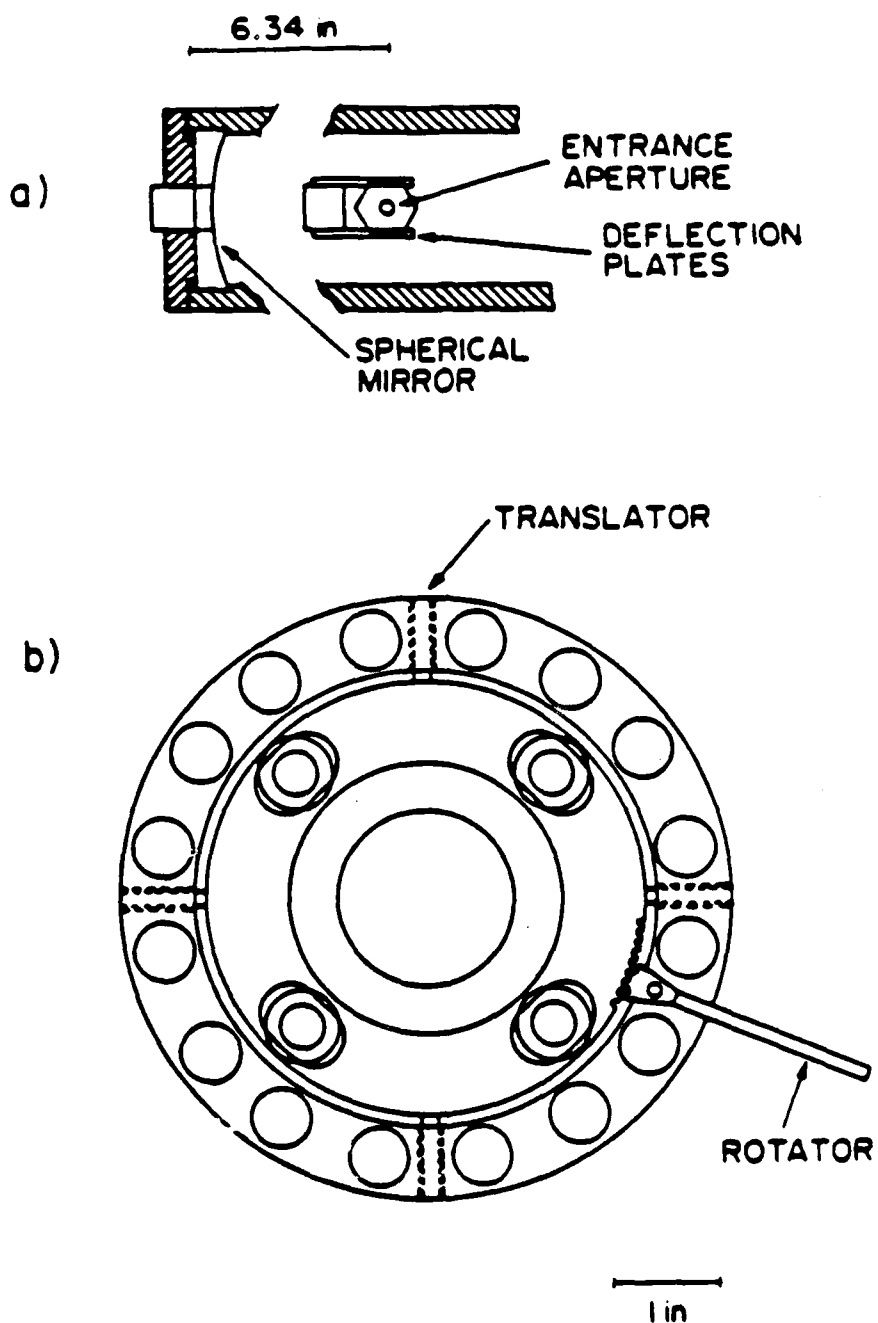


Figure 8. Vertical cut view of photoionization cell a) Side view of photoionization cell sighting through entrance aperture looking toward the mass spectrometer. The hatched areas indicate the cell walls. b) Front view of photoionization cell looking at it mounted on the viewport of the bell jar.

to disperse the emitted photons. Only photons having an energy corresponding to the energy difference between these two states will be detected. These changes should eliminate the large photon background which led to the failure of the early attempts to carry out these experiments.

2. EQUIPMENT DESIGN, CONSTRUCTION AND TESTING

2.1 Apparatus Description

The equipment used in these experiments consisted of an arc heated metastable H_3 beam source and a crossed molecular beam apparatus.

The H_3 beam source is depicted in Figure 9 , attached by a bellows to a vacuum chamber containing test mass spectrometric detection equipment. The performance of the source is indicated in the mass spectra of Figure 10., whose upper panel shows an intense peak at $m/e = 3$ due to the metastable H_3 species.

The crossed molecular beam apparatus is depicted in Figure 11 , which shows a supersonic primary beam source of hydrogen molecules (PB), a secondary beam capillary array (SB), and a rotatable mass spectrometer detector (MS), pumped by a liquid helium cryopump (CP) and a turbomolecular pump (TMP). A gate valve in front of the mass spectrometer entrance aperture is not shown for reasons of clarity of the diagram. During the course of this project, we have modified and joined these two major pieces of equipment. First, the crossed molecular beam apparatus was modified by removing entirely its primary beam source and corresponding internal vacuum enclosure (PB) of Figure 11. Second, the liquid helium cryopump (CP) was removed and replaced by another 360 l/s turbomolecular pump. With this change, continuous operation of the detector is now possible since recharging the cryopump with liquid helium is no longer necessary. Third, a Stern-Gerlach magnetic velocity selector was installed in its place, with a new vacuum box. Fourth, the arc source was detached from the test chamber (see Figure 9) and physically transported to the vicinity of the crossed molecular beam apparatus. Fifth, a coupling device was designed and constructed to connect the Stern-Gerlach magnetic velocity selector vacuum box to the arc

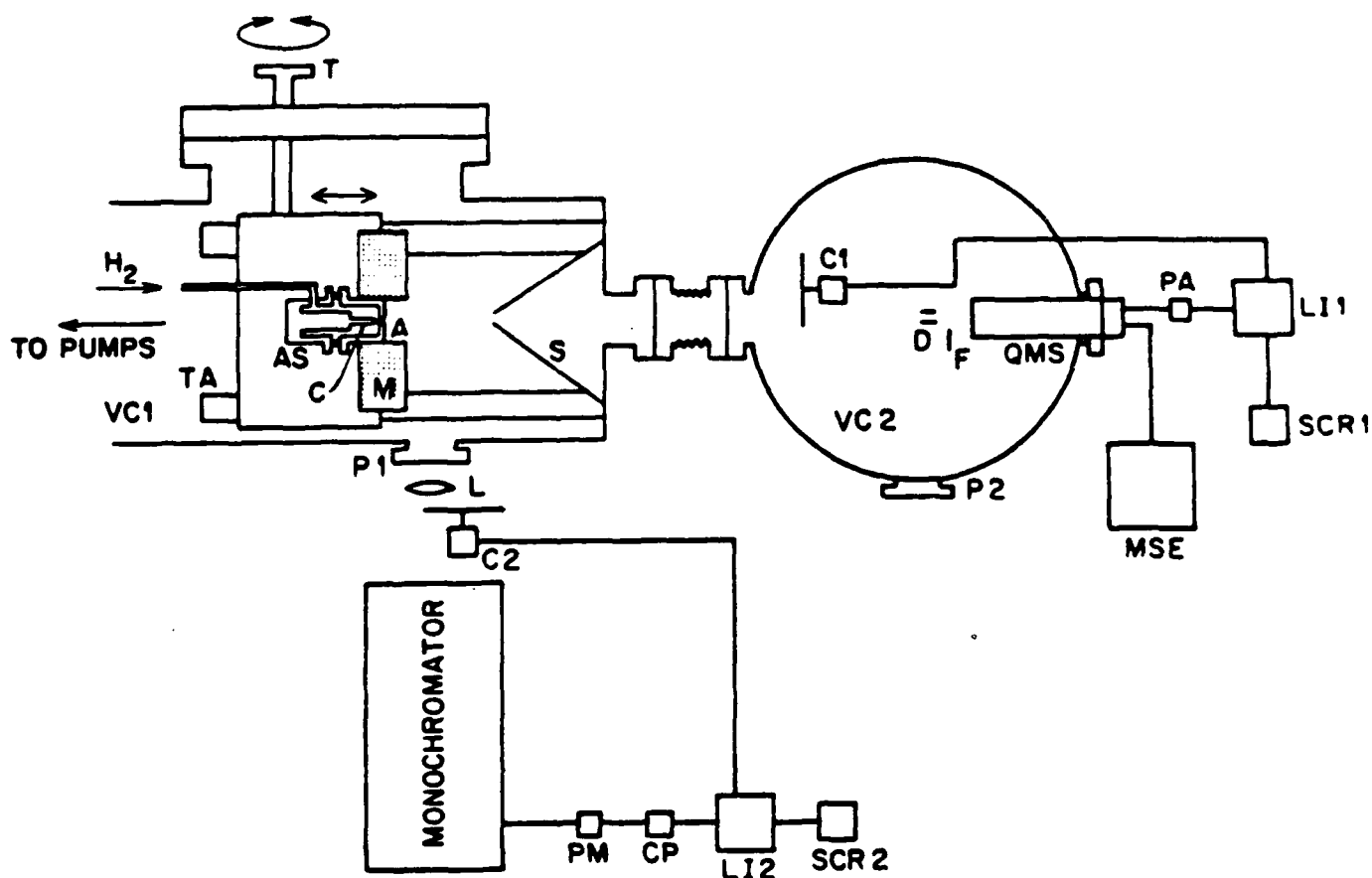


Figure 9. Schematic horizontal cut view of the apparatus used in the experiments in which the H_2 beam was tested: VC1 and VC2, vacuum chambers; AS, anode assembly; A, anode; C, cathode; M, magnet; S, water-cooled copper skimmer; TA, translation assembly; T, mechanical feedthrough translator; P1 and P2, viewports; L, optical lens; C1 and C2, choppers; D, electric field deflector plates; F, mechanical flag; QMS, quadrupole mass spectrometer; PA, preamplifier; MSE, mass spectrometer electronics; LI1 and LI2, lock-in amplifiers; SCR1 and SCR2, strip chart recorders.

source through the walls of the crossed molecular beam bell jar. Sixth, a gate valve was installed between the two major pieces of equipment which were then interconnected. This gate valve allows us to expose the source chamber to air while the crossed molecular beam apparatus is maintained under vacuum.

The resulting arrangement is depicted in Figure 12. A great deal of work was involved in appropriately aligning the two pieces of equipment with respect to one another.

To be able to perform the proposed experiments with the H_3 source, very nearly perfect beam alignment is necessary. However, when the beam was mechanically aligned using optical techniques, there was a small deviation between this optical alignment axis and the actual beam axis, of the order of 0.2° . Although small, this caused the beam to miss the center of a fixed aperture at the exit of the differential pumping chamber, 119 cm away, by about 4 mm. The cause of this misalignment was a slight difference between the optical axis and the magnetic axis of an electromagnet placed around the source, which varies from run to run by about $\pm 0.2^\circ$ and which drifts during the course of each run as source conditions change by about $\pm 0.2^\circ$. As a consequence of these results, it became obvious that until the arc source was modified so as to permit it to be moved during operation, scattering experiments would not be possible. An entirely new support structure was designed which provided 5 degrees of freedom (3 translations and 2 rotations) to the arc source during operation. However, the new design had the disadvantage that its dimensions were somewhat larger than the present one, and as a result would not fit in the existing vacuum chamber. This required construction of a new vacuum chamber. The design and construction of the arc source support structure and new vacuum chamber will be discussed later.

In order not to interrupt the progress of the scattering experiments while the new arc source support structure and chamber were being built, we had done two

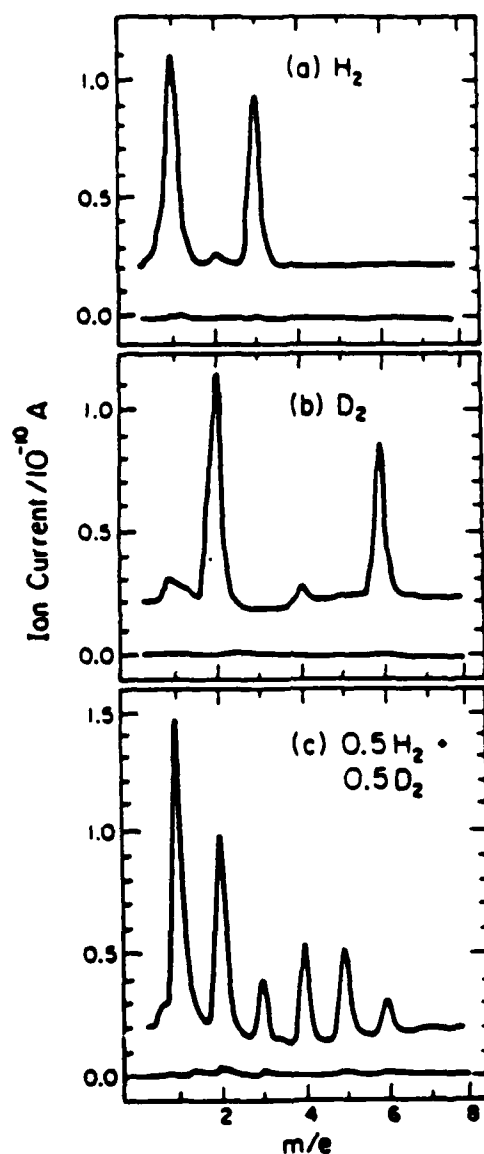


Figure 10. AC ion current as a function of m/e . In each panel the lower curve is the AC background obtained with the electron beam turned off, and the upper curve is the AC mass spectrometer ion current signal (with the beam chopped at 10 Hz) shifted upwards by 0.2×10^{-10} A for convenience of display. Electron impact current: 100 μ A. Electron accelerating voltage: 60 V. Ion source pressure: 2.1×10^{-5} torr measured by an uncalibrated ion gauge. (a) H_2 in the molecular beam source; (b) D_2 in that source; and (c) equimolar mixture of H_2 and D_2 in that source. For all panels the stagnation pressure in the molecular beam source was 60 torr. (Nozzle conditions changed slightly).

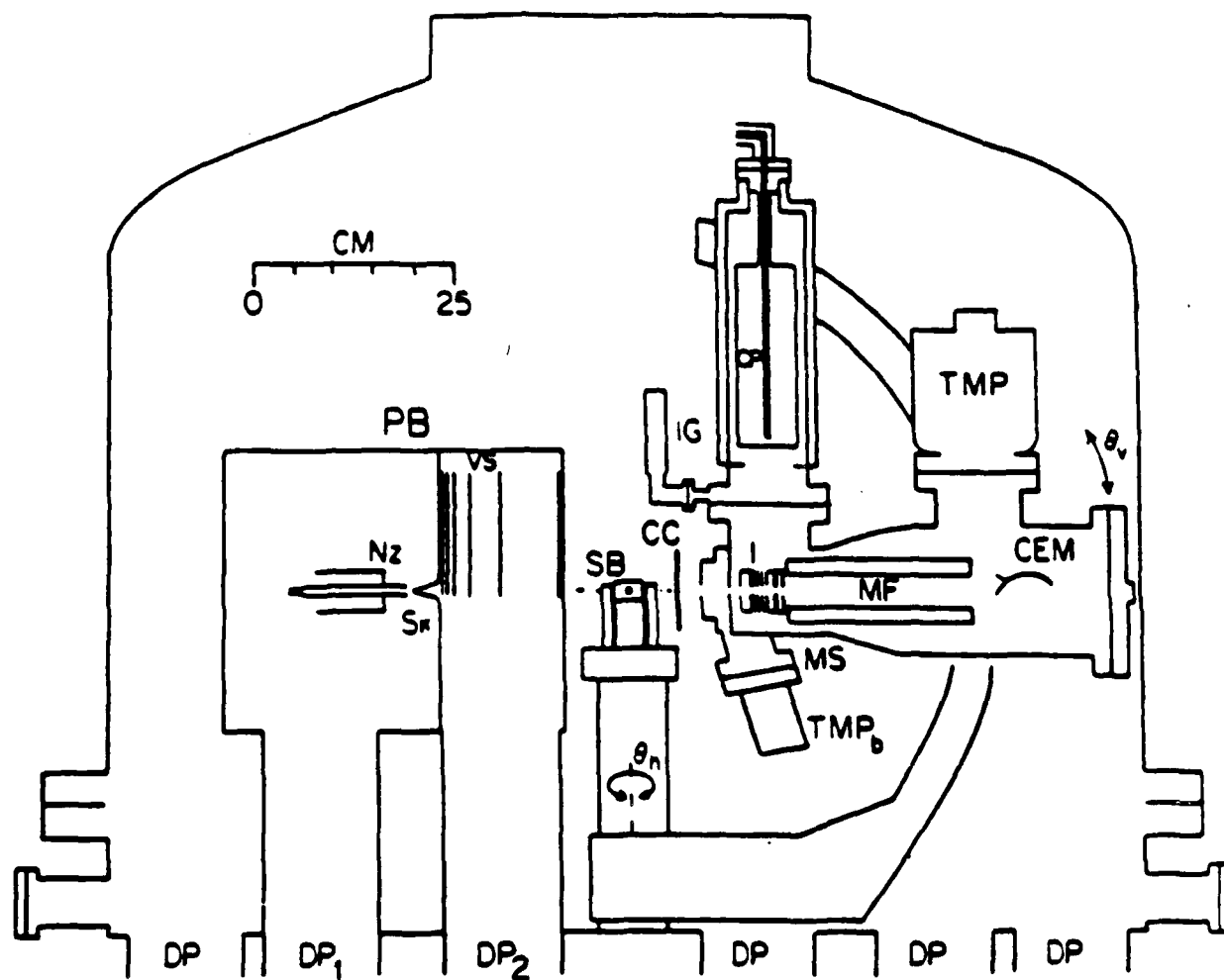


Figure 11. Vertical cut view of the crossed molecular beam apparatus, drawn approximately to scale. DP, diffusion pumps; PB, primary beam source (with the beam axis in the plane of the drawing); Nz, nozzle; SK, skimmer; VS, velocity selector; SB, secondary beam source (with the beam axis perpendicular to the plane of the drawing); CC, correlation chopper blade; MS, mass spectrometer detector; TMB_b, 50 l/s turbomolecular pump for buffer chamber; I, ionizer and ion-focus lenses; CEM, channeltron electron multiplier; CP, 350 l/s liquid He cryopump; TMP, 360 l/s turbomolecular pump; IG, ionization gauge.

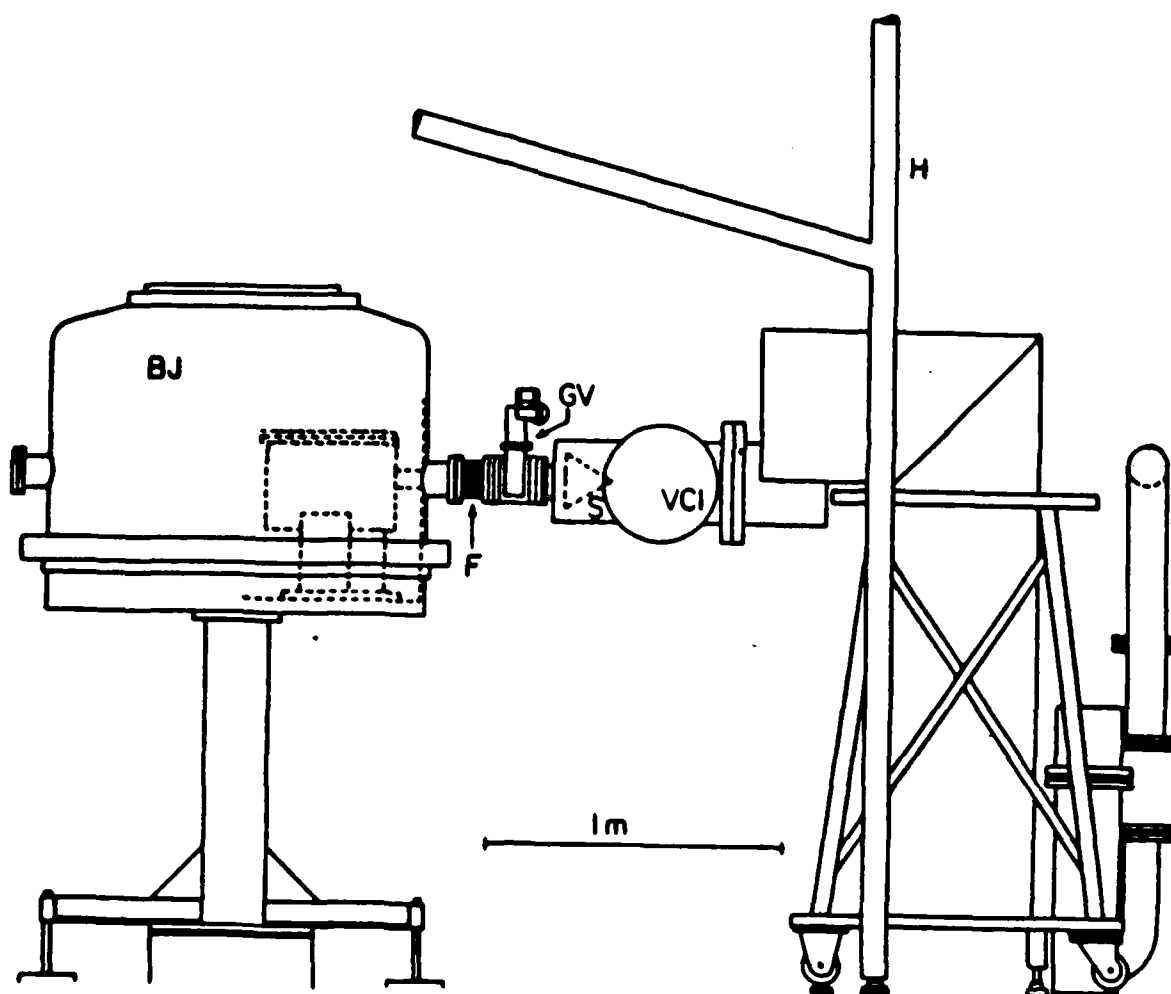


Figure 12. Side view of hybrid apparatus with metastable H_3 arc discharge primary beam source connected to the crossed molecular beam apparatus. VC1, vacuum chamber; S, water-cooled copper skimmer; GV, pneumatic gate valve; F, flexible metal bellows flange; BJ, 50" bell jar. Dashed lines indicate box within the bell jar which contains the magnetic velocity selector.

things. The first was to install a remotely controlled iris diaphragm at the exit of the magnetic velocity selector box. The second was to construct a pivot for the source chamber. Ideally, we wanted to move only the source and magnet, however due to the internal space limitations of the vacuum chamber VC1, this could not be done. Instead, the pivot is external and the source chamber can be rotated about a point directly below the center of the anode disk. The vacuum chamber and pump are mounted on a frame supported by 4 sturdy screws. The frame has been anchored to the concrete floor at the point directly below the center of the anode disk. With the help of horizontal screws threaded through heavy metal blocks anchored to the concrete floor, a horizontal force can be applied to the frames legs. The pivot causes the entire assembly to rotate around a vertical axis passing through the center of the anode disk. This motion can be applied while the source is operating. These changes have allowed us to produce the beam as usual and with the iris diaphragm fully open to locate it using the rotatable mass spectrometer. Once located, the pivot is used to move the chamber and therefore change the direction of the beam so as to bring it back as nearly as possible to the desired path. Once this has been achieved, the iris diaphragm is closed down to 2-3 mm so that the crossed beam experiments can be performed.

2.2 HI Beam Trap

In preliminary experiments done, HI was admitted to the capillary array beam source. After about 1 hour of operation, all exposed surfaces showed a rusty looking film due to either an I_2 impurity in the beam or reaction of some of the metal surfaces with HI. This required a thorough cleaning of the apparatus, including changing of the pumping fluids in all the diffusion pumps. In order to prevent this from happening in the future, we designed an HI beam trap. It

consists of a gate valve aligned with the secondary beam and a liquid-nitrogen-cooled stainless steel plate. About 98% of the HI will impinge on this plate, which should greatly decrease the contamination of the apparatus. In addition, the flow system for admitting gases into the secondary beam was modified. An additional trap was placed in the inlet line to remove condensable vapors, such as I_2 .

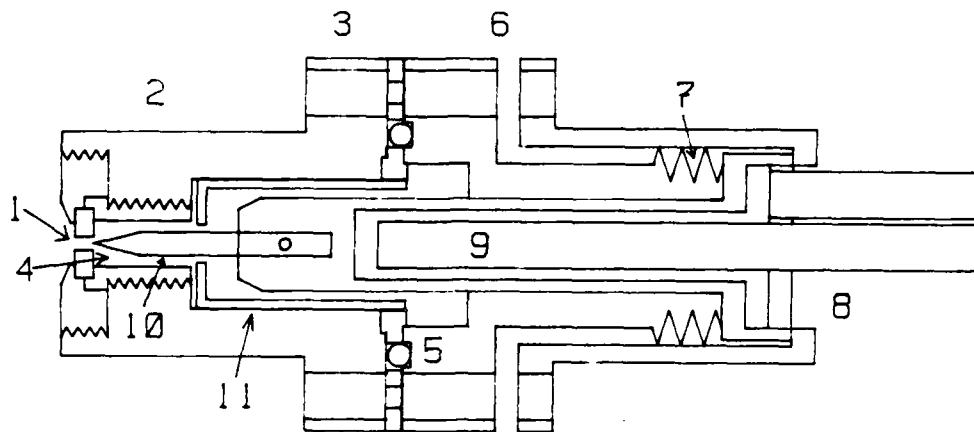
2.3 Maintenance

Extensive maintenance of the crossed beam apparatus was required. It involved disassembling, cleaning and reconditioning all 8 diffusion pumps and cryotrap of the apparatus, as well as the associated gate valves and vacuum plumbing. The mechanical pumps and the associated manifold and exhaust lines also had to be disassembled, cleaned and reinstalled. In addition, both turbomolecular pumps were cleaned and reconditioned. The mass spectrometer detector was also cleaned and reconditioned. The rest of the equipment inside the bell jar also had to be disassembled and cleaned. The entire apparatus was reassembled.

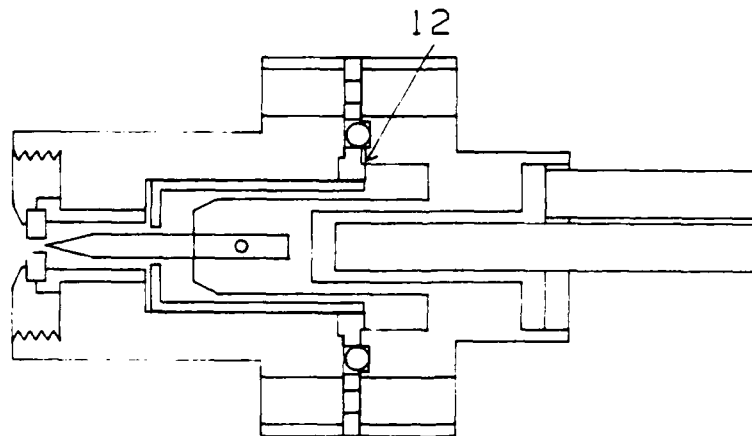
2.4 Arc Discharge Source

A cut away view of the arc heated source being used for these experiments is shown in Figure 13. This figure shows a) the source developed and used by Garvey and Kuppermann, and b) the source presently being used. As can be seen from this figure, several changes in the source have been made to improve the H_3 beam intensity, its reproducibility, and the duty cycle for these experiments.

The cathode portion of the source is shown in Figure 14. Parts a) and b) correspond to the same as in Figure 13. It is made up of a hollow stainless steel tube (A) with a $\frac{1}{8}$ " diameter tip cathode rod (B) attached to the front. The rod



a)



b)

Figure 13. Cut away view of arc discharge source a) Original source: 1, exit aperture; 2, anode housing; 3, water cooling inlet/outlet ports; 4, source gas chamber; 5, o-ring insulator and vacuum seal; 6, cathode support; 7, flexible bellows; 8, cathode; 9, cathode water cooling channel; 10, cathode tip; 11 macor cylinder. b) Modified source: 12, ceramic shoulder.

is made of 2% thoriaed tungsten and is capable of withstanding temperatures in excess of 3000 K. The tip of the tungsten rod is filed into the shape of a very dull pencil. During operation of the source, it tends to erode. The tungsten rod is attached to the base (D) using set screws. The cathode was originally equipped with a brass bellows (E) which allowed the cathode tip to move $\frac{3}{4}$ " with respect to the base. It is water-cooled to avoid heat damage. Two gas inlets are drilled at sharp angles through the base (D) on opposite sides. This tends to create a more stable flow through the nozzle by causing the gas to swirl around inside the source.

The bellows was originally included in the design so that the cathode tip to anode disk distance could be varied from experiment to experiment, so as to determine the optimum distance of separation. However, we found that the presence of the bellows made the source much less stable. It was found that tension in the cooling water lines connected to the cathode or a change in the water pressure to these lines caused the cathode to move. This produced a change in the discharge which in general decreased the intensity of the beam. In addition, the presence of the bellows also made the detected intensity of the beam less reproducible due to undesirable motion of the cathode tip. To eliminate this problem, the bellows was removed and the cathode tube was welded to the base. This change also allowed a decrease in the amount that the tungsten rod extended from the base, making it even more stable.

The anode assembly is shown in Figure 15. It is made up of a large cylindrical brass piece (D1 and D2) which has six water cooling channels bored into it. The nozzle assembly fits into the front of the brass housing. To avoid striking the arc in the anode housing, it is electrically insulated from the cathode everywhere except at the tungsten rod. This was achieved with a macor cylinder machined to cover the entire cathode tube except the rod as shown in Figure 15. The other

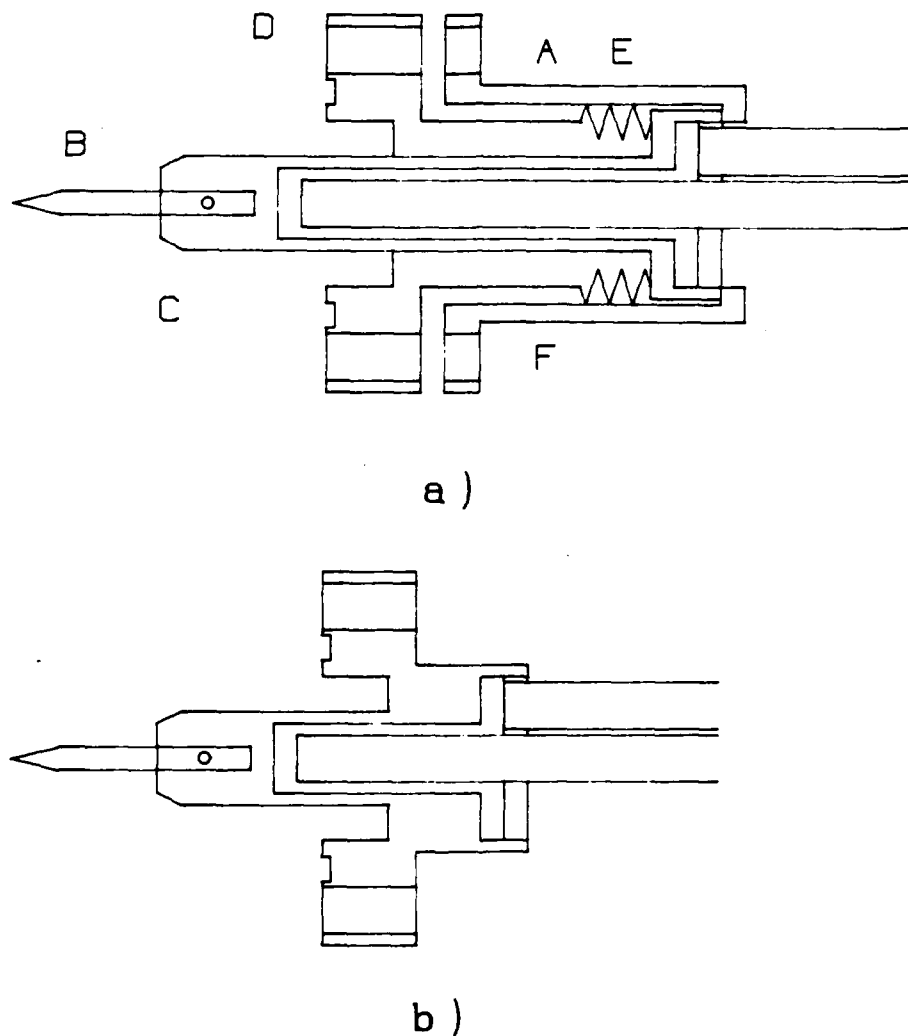
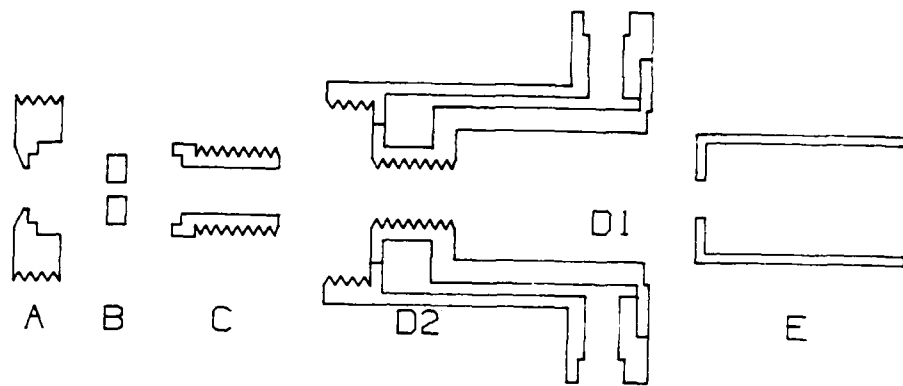


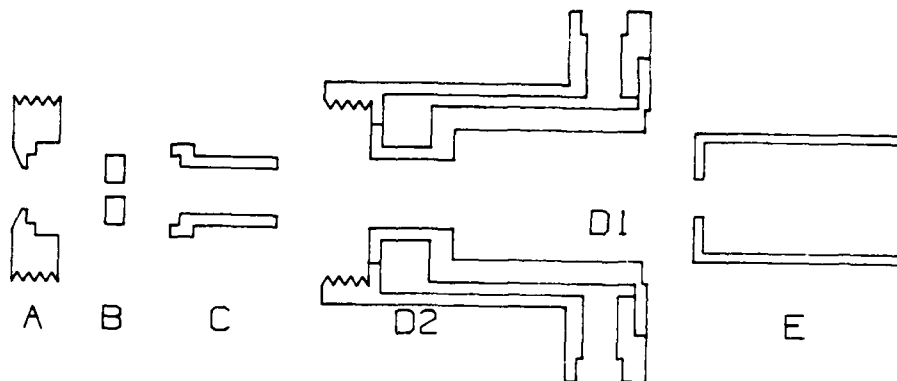
Figure 14. Scale drawing of cathode assembly a) Original cathode assembly: A, hollow tube; B, tungsten cathode rod; C, set screw; D, support structure; E, bellows; F, outer casing. The view of the cathode is a cross-sectional cut permitting a view of both sets of teflon screw holes in the support structure. The assembly is made out of stainless steel. b) Modified cathode assembly.

parts of the anode assembly are also shown in a disassembled configuration. The anode disk (D) is made of a $\frac{1}{8}$ " thick disk of tungsten which was cut from a $\frac{3}{8}$ " welder's rod. The disk has a 1.8 mm hole drilled into it. In the past, a 1.2 mm hole was used, however when this was tried, it was found to melt and close up during operation. Many size openings were tried until it was determined that 1.8 mm was the optimum opening. The disk was originally held in place by two copper pieces (A and C) which are threaded into the anode. However, the threads tended to cause the center opening to be off slightly thus making alignment more difficult. To produce a more accurate centering of these pieces, the threads were removed from the anode housing and the inner copper insert (C) and the pieces were machined to fit snugly in place.

When assembled, the anode and cathode were previously joined by six teflon screws; however, due to the lack of strength and the ease at which they were damaged, they were replaced by stainless steel screws. Bakelite washers and ceramic cylinders were used to provide electrical insulation. The cathode and anode are also electrically insulated from each other by a teflon spacer and a Viton o-ring which also provides a vacuum seal between them. In addition, a ceramic spacer has been placed in the center having shoulders on it to align the o-ring and inacor cylinder of the anode assembly. This helps to accurately center the cathode rod with respect to the anode disk and thus minimizes damage to the rod and disk during operation. Since these changes have been implemented, we have been able to run the discharge up to 8 times before replacing the cathode rod and anode disk. In addition, these changes have made it possible to run for longer periods of time, 14 hours being the longest we have tried. In the past, erosion of these pieces was significant enough to force us to change these parts after each run.



a)



b)

Figure 15. Exploded view of anode assembly a) Original anode assembly: A, threaded copper top; B, tungsten anode; C, threaded copper bottom; D (1 and 2) brass anode housing; E, macor[©] cylinder. b) Modified anode assembly: C, copper bottom.

Once assembled, the space between the tungsten rod and anode nozzle forms a small chamber (Figure 13 (4)) into which the gas may flow from the inlet lines (Figure 13 (3)). To prevent shorts, the cathode is insulated from the rest of the chamber by using $\frac{1}{4}$ " polyethylene tubing for the water lines, and by placing a glass spacer in the metal gas inlet line. The 'cathode tip-anode disk' distance was originally adjusted when assembled by compressing the cathode bellows (Figure 13 (7)). However, since the optimum gap between the tip of the cathode and the surface of the anode disk was found to be 0.5 mm, this distance is now always used. If in the future we wish to change this distance, it can be easily done by changing the length of the cathode rod used.

The source is mounted in the center of a 6" diameter by 1.4" thick electromagnet (M). Figure 16 shows the magnet (M) mounted on a moveable rail track. This translation assembly (TA) allows movement of the arc source and magnet during operation, permitting the nozzle to skimmer distance to be varied. This is achieved using a mechanical vacuum feedthrough translator (T) mounted on the 10" flange which provides access to the source chamber. However, the movement of the source using the translation assembly is very coarse and inaccurate due to slippage of the chain which transmits the translational motion. To eliminate this problem, the translation assembly was also redesigned to provide fine as well as accurate movements of the source. These changes will be discussed later.

It was found that during operation the direction of the beam changed. We initially attributed this to instabilities in the support structure and translation assembly of the source, created by heating of these elements during operation. To minimize this problem, we made changes that tightened the fitting of the source on the support structure. In addition, we bolted down the back of the magnet to make it less susceptible to changes produced by heating. We also bolted down the back

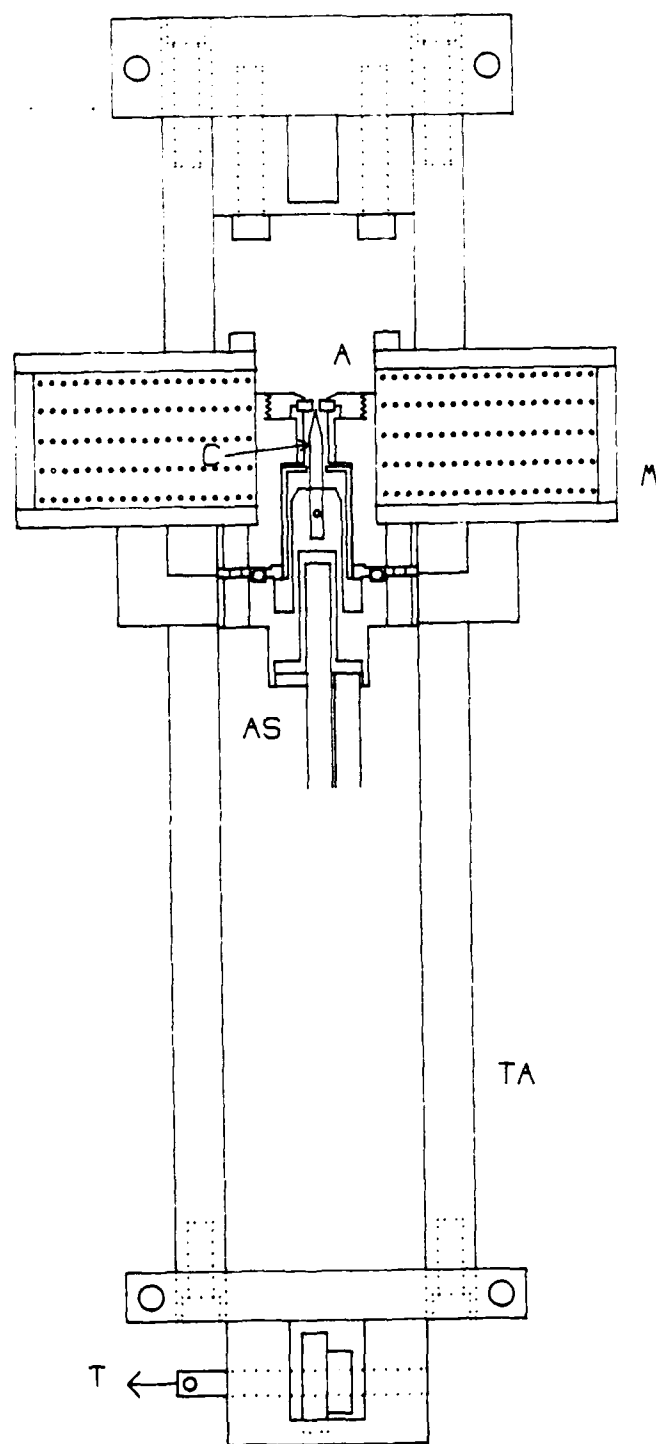


Figure 16. Schematic view of the top of the source, magnet and translation assembly. M, electromagnet; TA, translation assembly; T, translator; AS, anode assembly; A, anode; and C, cathode.

of the translation assembly to the source chamber to make it less susceptible to changes produced by vibrations of the pumps. To make the translation assembly of the source more reproducible, we replaced the translation support rods with ones which provided a tighter fit. Since these changes have been made, the direction of the beam has been more reproducible. However, it has not eliminated the problem.

As can be gathered from the above description, there still were problems with the source which had to be corrected before high quality results could be obtained. However, trying to incorporate these changes in the original source chamber was impossible due to the space limitations. Instead, we redesigned and built a new translation-rotation assembly for the source that is housed in a new source chamber.

2.5 Source Translation-Rotation Assembly

As discussed earlier, the major problem encountered in attempting to do crossed beam experiments with the H_3 beam is alignment. It has been found that when the H_3 beam is mechanically aligned using optical techniques, there is a small deviation between this optical alignment axis and the actual beam axis. The cause of this misalignment seems to be a slight difference between the optical axis and the magnetic axis of the electromagnet placed around the arc source, which varies slightly from run to run. In order to overcome this problem, we have designed and built a new translation-rotation assembly which allows us to correct this problem during operation of the source. This new assembly is pictured in Figure 17. This new assembly provides 5 degrees of freedom (3 translations and 2 rotations) to the source and magnet.

The design of the new translation assembly is similar to that previously used. It is made up of three main blocks. The front and rear blocks are attached via

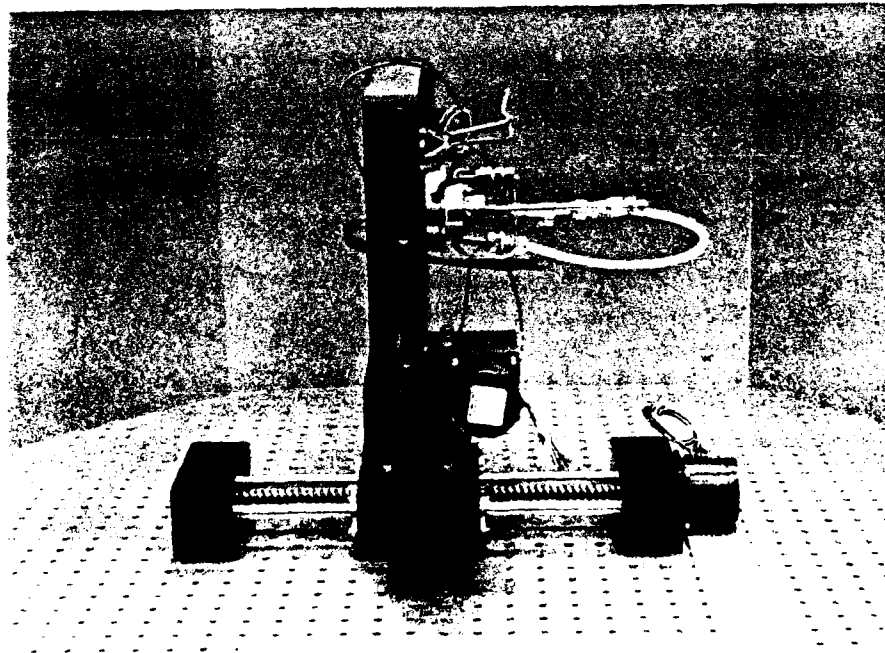
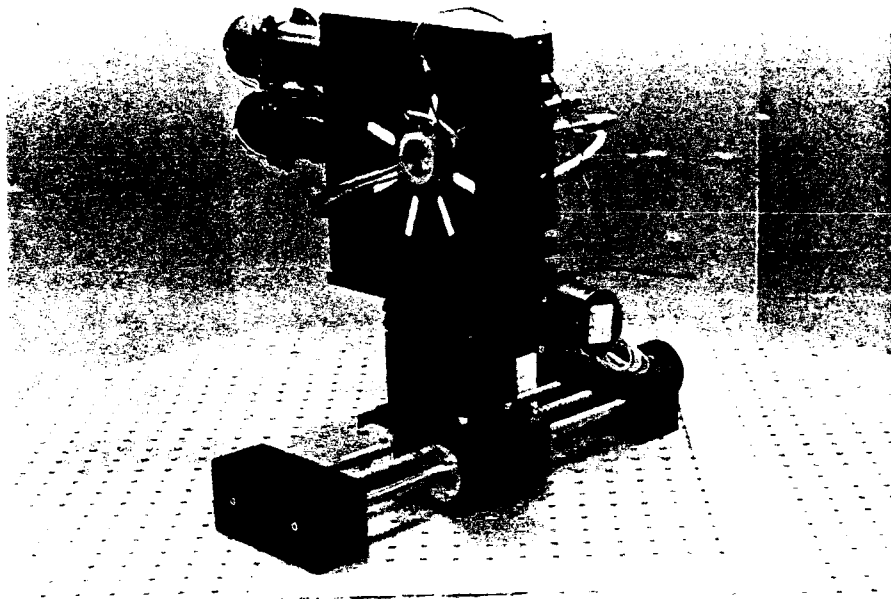


Figure 17. Side view of translation-rotation assembly.

two stainless steel rods and are secured to the bottom of the chamber providing a stable support structure for the entire assembly. The central block is moveable and supports the rest of the assembly. The motion is achieved using a motor driven screw. With this arrangement, we are able to achieve accurate movements of 0.0025" per step without backlash over a range of $> 8"$. Microswitches have been installed at the front and rear to provide stops to protect the motor from overwinding and to prevent damage to the skimmer.

The other two translations are provided by commercial translation stages. These have been mounted upon the central block of the other translation assembly. Motions are achieved through an ultra fine screw which has been coupled to a motor. Using these translation stages, we are able to achieve accurate movements of less than 0.0001" per step without backlash over a range of 1". Again microswitches have been installed to protect the motors from overwinding.

The two rotations are provided by a optical gimbal mount. It has been mounted on top of the uppermost translation stage. The magnet and source are mounted in it so that the gimbal point is located at the center of the anode disk. The gimbal mount was originally designed to hold very lightweight mirrors and had to be modified so that it could support the extra weight and tension created by the watercooling lines, the power lines, and the gas inlet line. In addition, retaining rings were made so that it could hold the source and magnet securely. With these modifications, the gimbal mount provides a stable and precise angular orientation of the source and magnet. Each of the motions are achieved through an ultra fine screw which has been coupled to a motor. Using the gimbal mount we are able to achieve accurate movements of less than 0.0003° per step without backlash over a range of 10° . Again microswitches have been installed to protect the motors from over winding.

As discussed above, the new translation-rotation assembly for the arc discharge source uses motors to drive each of the translations and rotations. To achieve these motions a electronics box to remotely control these motors and mircoswitches was designed and built. It allows the user to choose from the five degrees of freedom (3 translations and 2 rotations), the speed at which the motor will move (slow, normal or fast), the direction in which the motor will move (clockwise or counterclockwise), and it counts the number of steps taken. LED indicators have been used to inform the operator which motor has been selected, which speed has been selected, and when any of the limits has been reached.

2.6 Arc Discharge Source Control Panels

The new electrical control panel for the arc discharge source is shown in Figure 18. It allows for the operation of the source, and protects the source from damage in the event that something in the system does not operate properly. It is wired to an igniter which provides a high voltage pulse to start the arc. A Rentec 200 A lamp starter is used for this purpose. A Westinghouse arc welder power supply provides the voltage and current needed to sustain the arc. An arc welder power supply was mated with a 15 KVA, 3 phase, 60 Hz transformer (480V to 240V). The panel has a voltage meter and an ammeter which measure the voltage and current accross the arc. The panel allows one to raise or lower the arc current so that it can be maintained at 100 A throughout operation. The interlock system protects the source from damage by shutting off the arc power if: a) the pumping sytem is not turned on, b) the pressure in the chamber is too high, c) the skimmer temperature is too high, d) the flow of gas to the source is too low, e) the pressure in the source is too low, f) the cooling water flow to the source or magnet is too low, or g) if the temperature of the source is too high. It is

wired to a thermocouple gauge controller with an optical meter relay for chamber pressure measurement. It also has a temperature gauge which reads the skimmer temperature. It also allows one to remotely turn on the pumping system; the mechanical backing pump, the Roots blower or both.

The new gas flow panel for the arc discharge source is shown in Figure 19. It allows for the control and measurement of the flow of gas to the arc discharge source. It is connected to gas cylinders containing H_2 and Ar. Each has a separate inlet valve, fine metering valve, and a flow meter (0 to 150 ml/min for H_2 , and 0 to 10 SCFH for Ar) for measurement of the flow of each of these gases to the source. It has a valve to a mechanical pump which allows the system to be pumped out when setting up or shutting down the experiment. It also has a valve to open or shut off the flow of gas to the source. A Wallace and Tiernan pressure gauge (0 to 800 mm Hg) is used for measurement of the stagnation pressure to the source.

2.7 Source Chamber

As discussed above, the new translation-rotation assembly required more physical space than was available in the original source chamber. For this reason, a new source chamber was designed and built. It is shown in Figures 20 and 21.

The design of the new chamber eliminates many of the problems that existed in the original system, the most important of which are discussed below. The new chamber has a rectangular rather than a cylindrical shape. This eliminates the problem of the x-y directions being coupled and therefore makes alignment much easier. One of its sides can be removed, which facilitates access to the source, magnet and assembly for installation and servicing purposes. It has two view ports, which permit observation of the arc when the nozzle-to-skimmer distance is either large or small. This is important because the arc is ignited when this

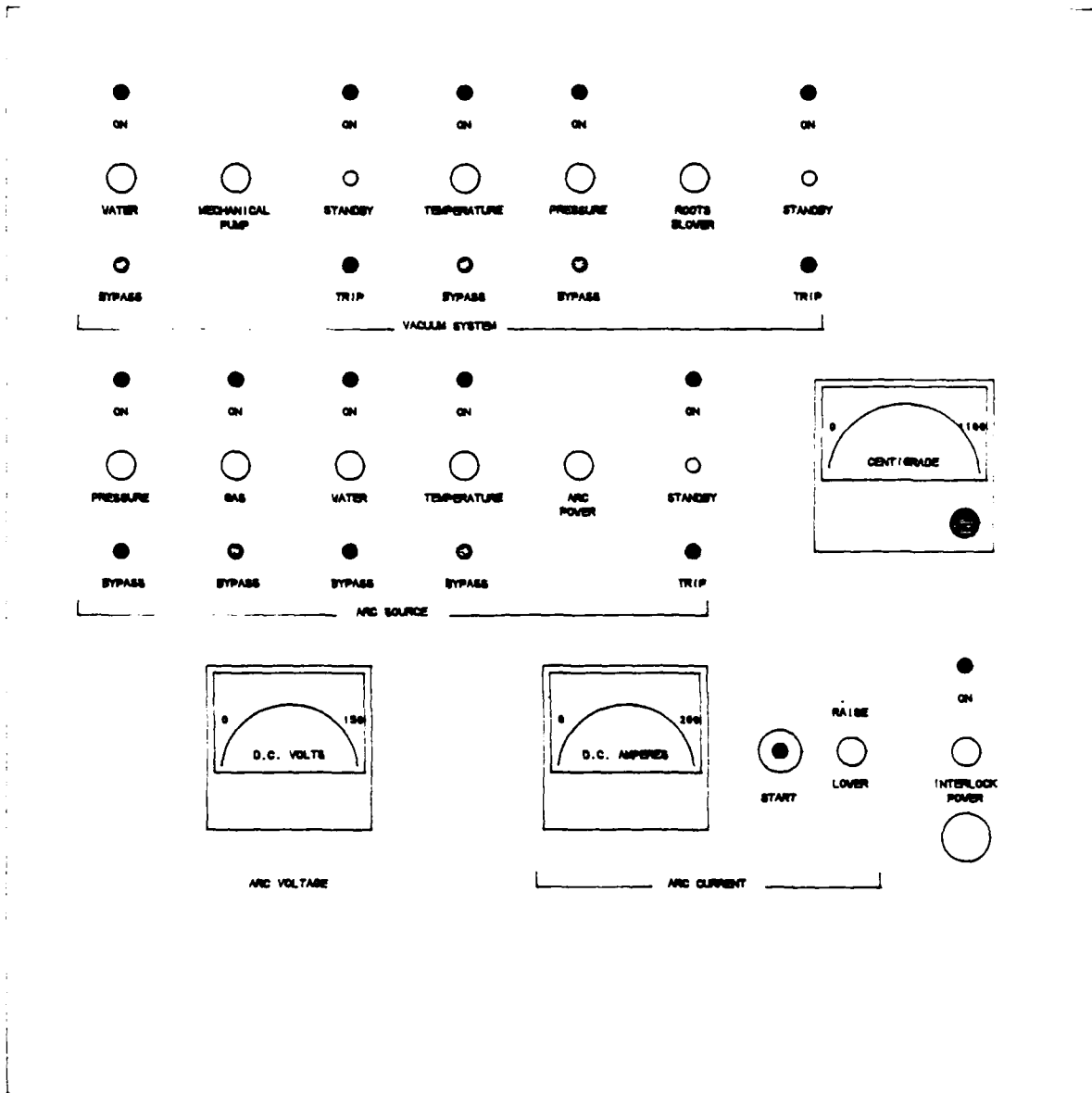
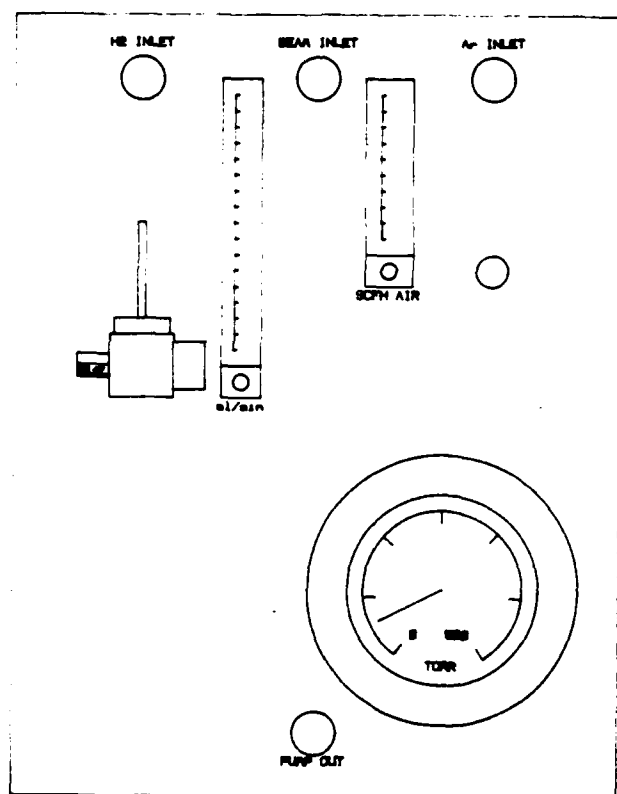
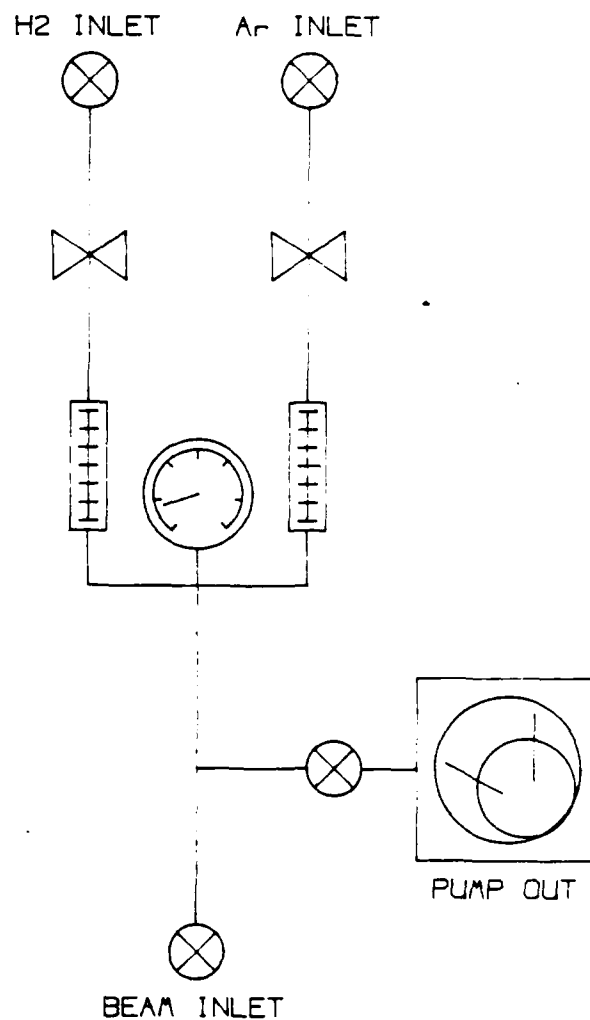


Figure 18. Schematic picture of the Arc discharge source electrical control panel

Filled circles indicate lights, and open circles indicate switches.



a)



b)

Figure 19. Schematic picture of the Arc discharge source gas flow panel.

a) Schematic picture of the front of the panel. b) Schematic drawing of the gas flow set-up.

distance is large, but during data collection this distance must be made small. The original enclosure only permitted visual observation during the ignition stage. The inside front face of the chamber was accurately machined to make it square with the base of the chamber. This squareness is crucial for the accurate alignment of the source with the rest of the system. In addition, positioning pins were installed to assure reproducibility of the position of the skimmer base after reassembly. This simplifies the alignment procedures.

Other important features of the chamber include: 7 feedthroughs (1 for power to the magnet, 1 for power to the arc source, 1 for water cooling lines, the gas inlet line and a temperature thermocouple, 2 for electrical connections between the motors of the translation-rotation assembly and the electronics box which controls their movement, 1 for a thermocouple gauge, and 1 for an ionization gauge), and 2 other ports (1 for the pumping system, and 1 for coupling to the other chambers of the system).

The source chamber is mated to a Roots pumping system through a flexible bellows mated to the port at the back of the source chamber. To minimize the transfer of vibrations created by the pumping system, a support system to fix the flex line in place was designed and constructed.

A stand was also designed to support the new source chamber. It rests on three alignment screws with leveling pads mounted on swivels whose angular degrees of freedom allow them to adjust automatically to unevenness of the floor. Since these alignment screws at the base of the stand provide only a coarse adjustment for alignment purposes, finer adjustment screws were placed at the top of the stand. In addition, there are screws which lock the chamber in place after alignment has been achieved. These features have improved the ease and stability of the beam alignment, which is a crucial characteristic. This stand has a

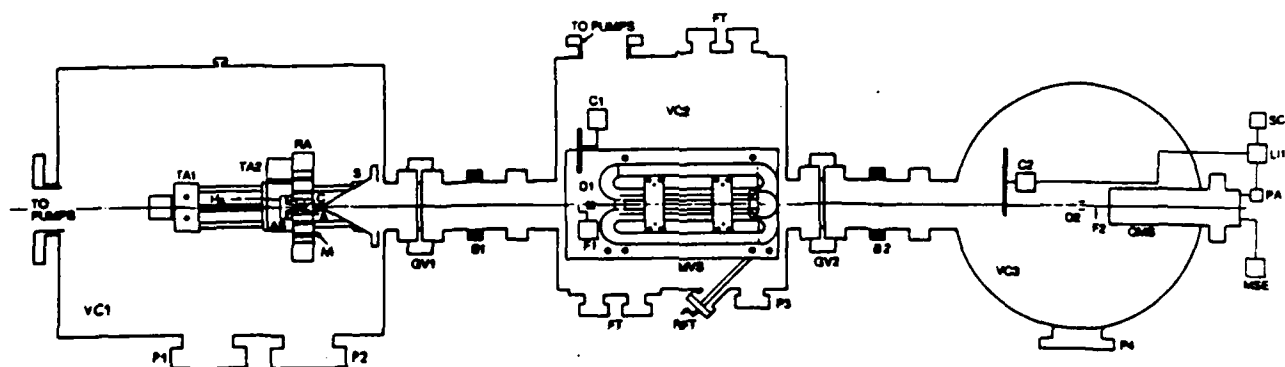


Figure 20. Horizontal cut view of apparatus used for H_2 experiments. VC1, VC2 and VC3, vacuum chambers; AS, anode assembly; A, anode; C, cathode; M, magnet; S, water-cooled copper skimmer; TA1 and TA2, translation assembly; RA, rotation assembly; P1, P2, P3 and P4, viewports; GV1 and GV2, gate valves; B1 and B2, flexible bellows; MVS magnetic velocity selector; FT, feedthroughs; RFT, rotary feedthrough; C1 and C2, choppers; D1 and D2, electric field deflector plates; F1 and F2, mechanical flag; FIP, field ionization plates; QMS, quadrupole mass spectrometer; PA, preamplifier; MSE, mass spectrometer electronics; LI1, lock-in amplifier; SCR1, strip chart recorder.

vertical extension so that the new source system can be used either in the crossed molecular beam apparatus or in the single beam apparatus.

2.8 Differential Stage Chamber

A new stage of differential pumping was designed and constructed for placement between the source chamber and the mass spectrometer vacuum chamber, to permit the latter to be operated at 10^{-7} torr pressure while the arc is on. In the original apparatus used for testing the H_3 beam source that pressure was in the 10^{-5} torr range, which is too high for the rovibrational population and lifetime measurements. It is shown in figures 20 and 21.

In addition to providing a differential stage of pumping between the source chamber and the mass spectrometer, the chamber was designed to house a Stern-Gerlach magnetic velocity selector. The design is similar to that of the box used in the crossed molecular beam apparatus for the same purpose. However since this new chamber is not housed in the bell jar as it is in the crossed beam apparatus, several changes in the design were made. First, the walls were made thicker due to the larger differential pressure between the interior and the exterior of the chamber. Second, it is pumped by only one mercury diffusion pump attached to the chamber through a flexible bellows which is connected to a side port. In the other system, two oil diffusion pumps are used to pump down the box with connection ports through the bottom of the chamber. Moving the vacuum port to the side improved the pumping speed since the magnetic velocity selector sits very close to the bottom of the chamber. Third, the entrance and exit ports were changed to 6" conflat for mating to the gate valves, flexible bellows and other chambers.

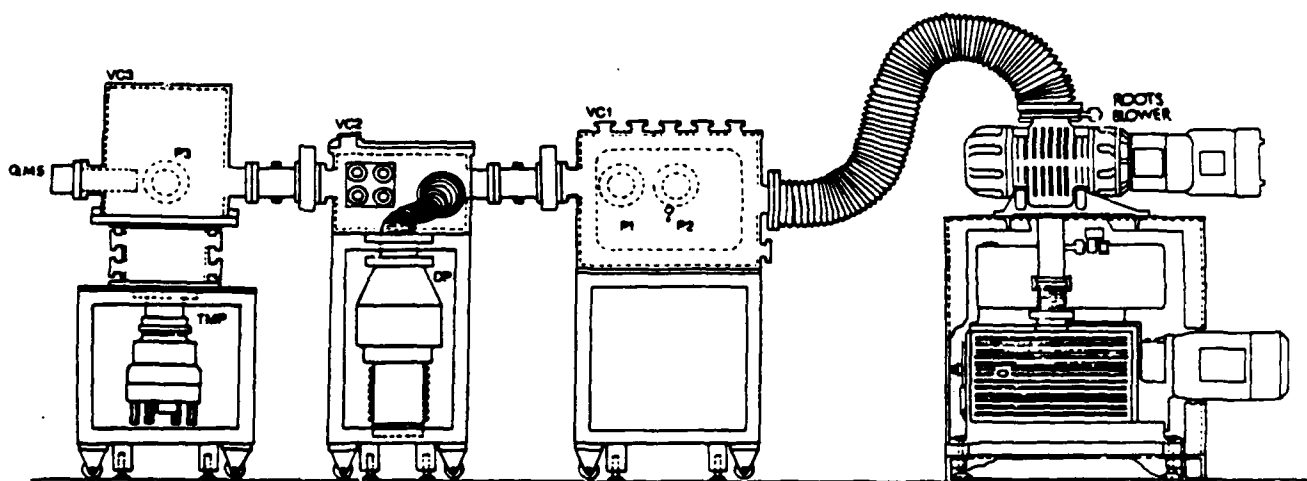


Figure 21. Vertical cut view of apparatus used for H_3 experiments. VC1, VC2 and VC3, vacuum chambers; P1, P2, and P3, viewports; QMS, quadrupole mass spectrometer; TMP, turbomolecular pump; DP, diffusion pump; Roots blower.

Other important features of the chamber include: 10 feedthroughs (1 for power to the magnet, 1 for cooling water for the magnet, 1 for air to the flag, 1 for power to the chopper, 1 for an ion gauge, 1 for the backing line manifold, 1 for power to motors for the slits, 1 viewport, 1 for the rotary motion feedthrough, and 1 spare). In addition, there are three leveling pads welded in the base of the interior for aligning the magnetic velocity selector and various mounts for the slits and motors.

A stand was also designed to support the new differential stage chamber. The design is similar to that used for the source chamber. Again, it rests on three alignment screws with leveling pads which provide a course adjustment, fine adjustment screws at the top of the stand for alignment purposes, and screws which lock the chamber in place after alignment has been achieved. The stand also supports a mercury diffusion pump and its cooling system.

2.9 Mass Spectrometer Vacuum Chamber

The vacuum chamber and its base used in the H_3 test system is also being used in the new system. It houses the mass spectrometer, a flag and deflection plates. In addition, the base provides 20 vacuum feedthroughs (only 6 of which are currently being used for voltage to the deflection plates, pressure/vacuum to the flag, an ion gauge, a thermocouple gauge, a sample gas inlet, and a vacuum relief valve. In the old system, this chamber (bell jar) was pumped by a mercury diffusion pump. A Leybold-Heraeus 360TMP turbomolecular pump equipped with a vent valve was purchased to replace this pump. The original pump purchased for this chamber was a grease-lubricated pump. However, it began to malfunction shortly after the warranty had expired. It was unable to pump down below 10^{-6} torr. The bearings were bad and had to be replaced. Since Leybold-Heraeus offered a buy out of this

pump, we traded it in for a more reliable oil-lubricated turbo pump of the same type (size and pumping speed). Since the mating flanges for the turbo pump and mercury diffusion pumps were different, a new adapter flange was designed and constructed. A Sargeant Welch model 1392 mechanical pump is used to back the turbo pump. A flexible backing line was designed to mate the backing pump to a valve and the backing port of the turbo pump.

A stand was also designed to support the bell jar. The design is similar to that used for the source and differential stage chambers. Again, it rests on three alignment screws with leveling pads which provide a coarse adjustment, fine adjustment screws at the top of the stand for alignment purposes, and screws which lock the chamber in place after alignment has been achieved. The stand also supports a mechanical hoist which allows raising or lowering the bell jar easily. A plate was also designed to mate the support loop on the top of the bell jar to the hoist. It has about 15 holes drilled through it to provide an adjustment in this connection so that the chamber can be maintained level when raising or lowering it no matter what is attached to the bell jar ports.

2.10 Mass Spectrometer

When we shifted to our studies on the properties of the metastable H_3 beam on a single beam apparatus, (see section 3) it had been two years since the corresponding mass spectrometer had been used. First it was disassembled and thoroughly cleaned. In the process of doing so, we found that several pieces were either damaged or missing. Most of these parts were spacers or shielding structures. New parts were either bought if available or machined otherwise. After thoroughly cleaning the mass spectrometer, the filament and electron multiplier were replaced. The electron multiplier that was installed was a solar blind one

with replaceable dynodes. Since it had been a while since it was used, the dynodes were changed before installation.

After refurbishing the mass spectrometer, we constructed and installed new and longer cables needed to connect it to the control circuitry which was placed at a larger distance.

In checking the control circuitry, we found that the preamplifier was not operating properly. We replaced it with one which worked. Both power supplies used for the electron multiplier (one for the x-ray shield and one for the high voltage) were not working properly and were repaired. The ionizer controller was not functioning properly. It was thoroughly refurbished. The radio frequency (RF) DC generator also had to be fixed. The mass spectrometer, as a result of all of these repairs, was made operational and tested with acetone, butane, toluene and air. It yielded appropriate mass spectra, but with poor resolution. Attempts to improve this resolution are under way.

2.11 Laboratory

In addition to all of the equipment bought or made, several changes in the laboratory were necessary to carry out the proposed experiments. First, a closed loop chilled water line was installed, since a cleaner and cooler water source was required for the laser and the arc source. Previously only normal tap water was available in the lab. Second, an exhaust line for the source chamber pumping system was installed in the laboratory. Previously, only a 2" exhaust line was available in the lab. Since the exhaust port on the Roots pumping system is over 4" in diameter a new line had to be installed. It permits the effluent gases (H_2 and Ar) to be vented to the roof of the building. Third, a new high pressure air line was installed. Two electropneumatic gate valves in the single beam system required

an air line pressure in the 75 to 100 psi range, but only a 30 to 40 psi air line was available in the lab. Fourth, threaded inserts (Red Devils) were installed in the concrete floor to provide a means of tying down each of the stands for the three chambers and the flex line support structure. Tie downs and supports were designed and constructed for this purpose, 3 for each stand.

2.12 Laser Photoionization System

A Quanta-Ray laser system was purchased for the H_3 and H_4 experiments. Important features of this system include: a 20 Hz Nd:YAG laser, a prism harmonic separator, a harmonic generator accessory, a Nd:YAG pumped pulsed dye laser, a side-pumped final amplifier assembly, a preamplifier assembly, a motor control interface, and an ultraviolet system (for wavelength extension). In addition, a 5' by 12' research series honeycomb laser table (with a rigid support system), an energy meter (with a 1.0 sq. in. energy probe and a serial to parallel interface), and various optics were purchased. A chilled water source was required for the laser; its construction is discussed in the section on changes made in the laboratory.

The laser system was tested. The basic system was working well, but the frequency doubling system had a very low conversion efficiency. The reason for this was the poor shape of the 532 nm laser beam. A conversion kit was ordered to improve this shape and achieve the desired laser intensity in the wavelength range of 225 nm to 217 nm (needed for the H_4 experiments). Due to installation of the conversion kit, it is now operating according to specifications in the ultraviolet region of the spectrum.

2.13 Computer System

An Everex 1800 10 MHz computer system was purchased for data collection. Important features of this system include: 1024 Kb RAM, 1.2 Mb floppy, 360 Kb floppy, 30 Mb 40 ms fixed disk, microenhancer EGA card, 10 MHz 80287 coprocessor, NEC multisync II color monitor, IBM proprinter II, and a H/P color pro plotter with enhanced graphics cartridge.

To interface the computer system with the experiment, a Microway A/D board and Unkelscope software were also purchased. Other software obtained include: DOS 3.3, Fortran, Jot, PLT2, and ZPLOT.

The A/D board was installed in the computer, and then the entire system was set up and tested. The computer was then connected to the campus network to permit data transfer to other computers on which data analysis will be performed.

In addition, circuitry for interfacing the mass spectrometer to the PC was designed and constructed.

3. EXPERIMENTS

The initial experimental effort was directed towards the detection of H_4 and an approximate determination of its lifetime. The apparatus used for these experiments is shown in Figure 12. After aligning the system, we first attempted to merely detect the H_3 beam. We encountered difficulties because there were a large number of very small openings through which the beam had to traverse in order to reach the mass spectrometer detector, and the H_3 beam was not following the optical alignment axis. Next we tried to enlarge the openings to detect the H_3 beam. Upon doing so we were able to detect the beam; however the necessary openings were so large that the differential pressures required for quality crossed beam experiments could not be achieved. To reduce this problem, several changes were made. A remotely controlled iris diaphragm was installed at the exit of the magnetic velocity selector box, and an external pivot to provide a rotation of the source chamber was constructed. Ideally we wanted to move only the source and magnet, but due to space limitations inside the source chamber this was not possible. With this set-up we were able to detect the beam, use the pivot to bring the beam as close as possible to the desired path and then close down the iris diaphragm and perform the crossed beam experiments. However, these improvements were not enough to allow quality crossed beam experiments to be carried out. We then began working on the source and its translation assembly trying to make it more reproducible. Several changes were made in the source and translation assembly which helped to improve its intensity and the reproducibility of the beam (see section 2.4).

After the stability, angular width and intensity of the H_3 beam were optimized as best as possible within the limitations of its characteristics, crossed beam

experiments with Ar and HI were performed. In some experiments scattered H_3 molecules and H atoms were detected and in others they were not. This difference in results was caused by the drift in the position of the H_3 beam during the course of the experiment as well as changes that occurred from day to day. The reason for no scattered species to be detected, was that the angular tail of the primary beam was more intense than the signal due to scattered species. Since the drift in the H_3 incident beam intensity made it impossible to achieve reproducible results and because Montgomery et al.¹⁰ showed that H_4 was not bound, our efforts were redirected towards the improvement and characterization of the H_3 beam.

Most of the experimental effort after this point was directed towards the design, construction and testing of the apparatus to be used for the characterization of the H_3 beam. The results of the attempts to perform crossed beam experiments made it obvious that it was necessary to design and construct a translation-rotation assembly for the source to provide the 5 degrees of freedom needed to achieve accurate alignment of the beam with the optical axis during operation of the source. Such an assembly was designed, and built (see section 2.5). An electrical control box was also designed and built to control this assembly. The system was assembled and tested. Once the bugs were cured, we began working on a new chamber to house the source. A new source chamber and stand was designed, and built. During its construction, control panels were designed and built to control the source as well as all other needed parts for the system. Once the chamber was finished, the system was assembled and tested. Many problems were encountered, fixed and rechecked until the source could be operated properly and reproducibly.

Next, a new stand was designed and built for the bell jar. During its construction, other parts needed were designed and built. Upon completion, the

system was assembled and tested. Problems were diagnosed and cured. However, the mass spectrometer gave us a great deal of trouble. While trying to repair the mass spectrometer and its electronics, a differential stage chamber and stand was designed and built. In addition, all other parts needed for this chamber were designed and built. Upon completion, the system was assembled and tested. Again, problems were encountered and fixed one at a time until the system operated properly. Once this had been achieved, attention was turned back to the mass spectrometer. Each of its components were tested and repaired. The mass spectrometer is now functional but its resolution still needs improvement.

While all of these changes were taking place, a computer system for data collection was acquired, set up and tested. Appropriate software was acquired and tested. In addition, circuitry for interfacing the computer with the mass spectrometer was designed, built and tested. A laser system was also acquired, set up and tested for the spectroscopy experiments. Once we improve the resolution of the mass spectrometer to an acceptable level, we will initiate the rovibrational population measurements.

4. CONCLUSIONS

A sophisticated apparatus to produce and characterize a metastable beam of H_3 molecules was designed, constructed and assembled. It consists of an arc-heated metastable H_3 beam source, a Stern-Gerlach magnetic velocity selector and an electron bombardment mass spectrometer detector. The resolution of the latter still needs improvement. Once this is achieved, experiments will be performed to determine the rovibrational composition, translational energy distribution, and radiative lifetime of the metastable H_3 beam and to determine its chemical properties.

5. REFERENCES

1. Rosen, G., "Current Status of Free Radicals and Electronically Excited Metastable Species as High Energy Propellants," Jet Propulsion Laboratory report TR JPL 73-153.
2. Garvey, J. F., and Kuppermann, A., "An Intense Beam of Metastable H_3 Molecules," Chemical Physics Letters, Vol. 107, No. 6, pp. 491-495, June 15, 1984.
3. Garvey, J. F., and Kuppermann, A., "Design and Operation of a Stable Intense High-Temperature Arc-discharge Source of Hydrogen and Metastable Trihydrogen Molecules," Review of Scientific Instruments, Vol. 57, No. 6, pp. 1061-1065, June 1986.
4. Helm, H., "Observation of High- n Rydberg Series ($7 < n < 40$) of the H_3 Molecule," Physical Review Letters, Vol. 56, No. 1, pp. 42-45, January 6, 1986.
5. Cosby, P. C., and Helm, H., "Photodissociation of Triatomic Hydrogen," Physical Review Letters, Vol. 61, No. 3, pp. 298-301, July 18, 1988.
6. Helm, H., "Measurement of the Ionization Potential of Triatomic Hydrogen," Physical Review A, Vol. 38, No. 7, pp. 3425-3429, October 1, 1988.
7. Helm, H., Lembo, L. J., Cosby, P. C., and Huestis, D. L., "Photoionization and Dissociation of the Triatomic Hydrogen Molecule," in Fundamentals of Laser Interactions, Springer Verlag, 1989.
8. Nicolaides, C. A., Theodorakopoulos, G., and Petsalakis, I. D., "Theory of Chemical Reactions of Vibronically Excited $H_2(B^1\Sigma_u^+)$ I. Prediction of a Strongly Bound Excited State of H_4 ," Journal of Chemical Physics, Vol. 80, No. 4, pp. 1705-1709, February 15, 1984.

9. Kuppermann, A., entitled Tetrahydrogen, AFRPL-TR-86-103, January 1987.
10. Montgomery, J. A. Jr., and Michels, H. H., "On the Stability of H_4 in C_{3v} Symmetry," Journal of Chemical Physics, Vol. 86, No. 10, pp. 5882-5883, May 15, 1987.
11. Hehre, W. J., Radom, L., Schleyer, P. von R., and Pople, J. A., Ab initio Molecular Orbital Theory, Wiley-Interscience, New York, 1986.
12. a) Herzberg, G., "A Spectrum of Triatomic Hydrogen," Journal of Chemical Physics, Vol. 70, No. 10, pp. 4806-4807, May 15, 1979; b) Dabrowski, I., and Herzberg, G., "The Electronic Emission Spectrum of Triatomic Hydrogen.I. Parallel Bands of H_3 and D_3 Near 5600 and 6025 Å," Canadian Journal of Physics, Vol. 58, No. 8, pp. 1238-1249, August 1980; c) Herzberg, G., and Watson, J. K. G., "The Electronic Emission Spectrum of Triatomic Hydrogen.II. Perpendicular Bands Near 7100 Å," Canadian Journal of Physics, Vol. 58, No. 8, pp. 1250-1258, August 1980; d) Herzberg, G., Lew, H., Sloan, J. J., and Watson, J. K. G., "The Electronic Emission Spectrum of Triatomic Hydrogen.III. Infrared Perpendicular Bands Near 3600 cm^{-1} ," Canadian Journal of Physics, Vol. 59, No. 3, pp. 428-440, March 1981; e) Herzberg, G., Hougen, J. T., and Watson, J. K. G., "The Electronic Emission Spectrum of Triatomic Hydrogen. IV. Visible Bands Near 5800 Å and Infrared Bands Near 3950 cm^{-1} ," Canadian Journal of Physics, Vol. 60, No. 9, pp. 1261-1284, September 1982.
13. Karplus, M., and Porter, R. N., Atoms and Molecules: an Introduction for Students of Physical Chemistry, Benjamin/Cummings Publishing Co., 1970. p. 139.
14. Devienne, F. and Rousteau, J., "Physique Moléculaire-Détermination de l'existence et de certaines propriétés de jets moléculaire triatomiques d'hydrogène," Comptes Rendues Académie Des Sciences Paris Serie B: Science Physiques,

Vol. 263, No. 25, pp. 1389-1392, December 19, 1966.

15. Devienne, F. M. a) "Physique Molculaire-Existence et proprietes de jets molculaires triatomiques d'deuterium," comptes Rendus Academie Des Sciences Paris Serie B: Science Physiques, Vol. 264, No. 20, pp. 1400-1407, May 17, 1967; b) "Physique Molculaire-Preuve de l'existence de molecules triatomique dans un jet molculaire obtenu par exchange de charge d'un faisceau d'ions d'hydrogene triatomique." *ibid*, Vol. 267, No. 23, pp. 1279-1281, December 4, 1968; c) "Physique Molculaire - Ionisation par chocs inelastiques d'un jet molculaire triatomique d'hydrogene de haute energie sur une cible de deuterium." *ibid*, Vol. 268, No.20, pp. 1303-1306, May 19, 1969; d) "Experimental Study of Ionization of H_3^0 by Inelastic Collisions with Deuterium." Sixth International Conference on the Physics of Electronic and Atomic Collision, Massachusetts Institute of Technology, Cambridge, Massachusetts, pp. 789-791, 1969.
16. Gray, J. and Tomlinson, R. H., "Molecular Beam Studies of HeH and H_3 Molecules," Chemical Physics Letters A, Vol. 4, No. 5, pp. 251-254. November 15, 1969.
17. Barnett, C. F. and Ray, J. A., "Highly Excited States of Hydrogen Molecules II. H_3 ," Physical Review A, Vol. 5, No. 5, pp. 2120-2122, May 1972.
18. Nagasaki, T., Doi, H., Wada, K., Higashi, K., and Fukuzawa, F., "Experimental Evidence for the Existence of Tri-Atomic Hydrogen Molecules," Physics Letters, Vol.38A, No. 6, pp. 381-382, March 13, 1972.
19. Castro de Faria, N. V., Gaillard, M. J., Poizat, J.C., and Remillieux, J., "Observations of Mev H_3 Molecules," Annals of the Israel Physical Society, Vol. 4, 1981. Molecular Ions, Molecular Structure and Interaction with Matter. Published by Adam Hilger, Bristol and the Israel Physical Society in Association with The American Institute of Physics, New York, pp. 134-136.

20. Gaillard, M. J., Pinho, A. G. de, Poizat, J. C., Remillieux, J., and Saoudi, R., "Experimental Study of the Triatomic Hydrogen Molecule through the Collisional Sequence $H_3^+ \rightarrow H_3 \rightarrow H_3^+$ Undergone by Fast Beams in Argon," Physical Review A, Vol. 28, No. 3, pp. 1267-1275, September 1983.
21. Vogler, M. "Observation of an Electronically Excited State of H_3 and Determination of Its Vibrational Level Structure," Physical Review A, Vol. 19, No. 1, pp. 1-5, January 1979.
22. Cisneros, C., Alvarez, I., Garcia, R., Barnett, C. F., Ray, J. A., and Russek, A., "Electron Capture to D_3^+ in C_8 ," Physical Review A, Vol. 19, No. 2, pp. 31-40, February 1979.
23. Gellene, G. I., Cleary, D. A., and Porter, R. F., "Stability of Ammonium and Methylammonium Radicals from Neutralized Ion Beam Spectroscopy," Journal of Chemical Physics, Vol. 77, No. 7, pp. 3471-3477, October 1, 1982.
24. Gellene, G. I., and Porter, R. F., "Experimental Observations of Excited Dissociative and Metastable States of H_3 in Neutralized Ion Beams," Journal of Chemical Physics, Vol. 79, No. 12, pp. 5975-5981, December 14, 1983.
25. Figger, H., Moller, H., Schrepp, W., and Walther, H., "Laser Spectroscopy of D_3 ," Chemical Physics Letters, Vol. 90, No. 2, pp. 90-94, July 23, 1982.
26. King, H. R., and Morokuma, K., "Theory of the Rydberg Spectrum of Triatomic Hydrogen," Journal of Chemical Physics, Vol. 71, No. 8, pp. 3213-3220, October 15, 1979.
27. Kulander, K. C., and Guest, M. F., "Excited Electronic States of H_3 and Their Role in the Dissociative Recombination of H_3^+ ," Journal of Physics B: Atomic and Molecular Physics, Vol. 12, No. 16, pp. L501-L504, August 1979.
28. Way, K. R., Yang, S.-C., and Stwalley, W. D., "Arc-Heated High Intensity Source of Hydrogen Atoms," Review of Scientific Instruments, Vol. 47, No. 9, pp. 1049-1055, September 1976.

29. Garvey, J. F., and Kuppermann, A., "Total Scattering, Surface Ionization and Photoionization of a Beam of H_3 Metastable Molecules." Journal of Chemical Physics, Vol. 86, No. 12, pp. 6766-6781, June 15, 1987.
30. Martin, R. L., "Rydberg States of H_3 ," Journal of Chemical Physics, Vol. 71, No. 8, pp. 3541-3542, October 15, 1979.
31. Jungen, M., "Rydberg States of H_3 ," Journal of Chemical Physics, Vol. 71, No. 8, pp. 3540-3541, October 15, 1979.
32. Calzaferri, G., "The Instability of H_3 ," Chemical Physics Letters, Vol. 87, No. 5, pp. 443-446, April 9, 1982.
33. Tennyson, J., "The Ground State of H_3 Molecule," Chemical Physics Letters, Vol. 86, No. 2, pp. 181-184, February 12, 1982.
34. Raynor, S., and Herschbach, D. R., "Diatomics-in-Molecules Approximation for Rydberg States of H_3 ," The Journal of Physical Chemistry, Vol. 86, No. 7, pp. 1214-1217, April 1, 1982. "Electronic Structure of Rydberg States of H_3 , NeH, H_2F , H_3O , NH_4 , and CH_5 Molecules," The Journal of Physical Chemistry, Vol. 86, No. 18, pp. 3592-3598, September 2, 1982.
35. Hirao, K., and Yamake, S., "Theoretical Study of the Structure and Stability of Hydrogen-Ion Clusters H_n^+ and H_n ($n=3,5,7,9,11,13$)," Chemical Physics, Vol. 80, pp. 237-243, 1983.
36. Helm, H., (repeated calculation of King and Morokuma using a more accurate $2s^2A'_1$ to $2p_x^2A''_2$ gap of 898 cm^{-1}) to be published.
37. Levine, R. D., and Bernstein, R. B., in Molecular Reaction Dynamics, Oxford University Press, NY, 1974. pp. 213-216.
38. Herzberg, G., Molecular Spectra and Molecular Structure III: Electronic Spectra and Electronic Structure of Polyatomic Molecules, Van Nostrand Reinhold Co., New York pp. 45, 128ff., 298, 1966.

39. Bethe, H. A., and Salpeter, E. E., in Quantum Mechanics of One- and Two-Electron Atoms, Springer-Verlag, Berlin, 1957.
40. Stebbings, R. F., Latimer, C. J., West, W. P., Dunning, F. B., and Cook, T. B., Physical Review, Vol. A12, pp. 1453, 1975.
41. Allen, L., Jones, D. G. C., and Schofield, D. G., Journal of the Optical Society of America, Vol. 59, pp. 842, 1969.